Both edges of the EGFP-positive EMCs and MMCs along the line (Figs. 1L, 3K) were automatically detected, and the distance between both edges was measured from each video frame using an image edge-detection program using Igor Pro 4 (Wavemetrics Inc., Lake Oswego, OR) [11].

Calculation of Induction Rate

The MMCs and EMCs were exposed to 3 μM 5-azacytidine (5-azaC; Sigma-Aldrich) for 24 hours to induce cell differentiation, or were left untreated. The 5-azaC-treated and nontreated MMCs or EMCs, cultivated with or without murine fetal cardiomyocytes, were enzymatically dissociated and stained, then observed by confocal laser microscope (supplemental online data 2 for detail of method). The cardiomyogenic induction rate (average of 10 separate experiments) was calculated as the fraction of cardiac troponin-I-positive cells in the EGFP-positive cells.

Examination of Chromosomes of MMCs or EMCs and Murine Cell Chimeras

To rule out cell fusion-dependent cardiomyogenesis, chromosomes from MMCs or EMCs cocultivated without separation by the atelocollagen membrane from murine cardiomyocytes for 1 week were stained using a human chromosome-specific probe and a mouse chromosome-specific probe (Chromosome Science Labo, Hokkaido, Japan, http://www.chromoscience.jp/en/probe/page01/page01e.html) and spectral karyotyping with fluorescent in situ hybridization chromosome painting technique (Applied Spectral Imaging, Vista, CA, http://www.spectral-imaging.com), according to the manufacturer's protocol.

RNA Extraction and RT-PCR

Reverse transcriptase polymerase chain reaction (RT-PCR) was done as described previously [2]. Primers for the following genes were used: cardiac transcription factors—Csx/Nkx-2.5 and GATA4; cardiac hormones—atrial natriuretic peptide and brain natriuretic peptide; cardiac structural proteins—cardiac troponin I, cardiac troponin T, myosin light chain-2a, myosin light chain-2v, and cardiac-actin; and ion channel—cyclic nucleotide-gated potassium channel 2 (supplemental online Table 1). The internal control was 18S rRNA. PCR primers were prepared such that they would amplify the human but not the mouse genes.

Flow Cytometric Analysis

The cells were analyzed using an EPICS ALTRA analyzer (Beckman Coulter, Fullerton, CA, http://www.beckmancoulter.com). Antibodies (anti-human CD10, CD13, CD14, CD24, CD29, CD31, CD34, CD44, CD45, CD54, CD55, CD59, CD71, CD73, CDw90, CD105, CD106, CD117, CD133, CD140a, CD166, CD309, HLA-ABC, and HLA-DR) [12] were purchased from Beckman Coulter, Immunotech (Luminy, France, http://www.beckmancoulter.com/products/pr_immunology.asp), Cytotech (Hellebaek, Denmark, http://www.cytotech.dk/index.html), Santa Cruz Biotechnology Inc. (Santa Cruz, CA, http://www.scbt.com), RDI (Research Diagnostics, Inc., Concord, MA, http://www.researchd.com), and Pharmingen Pharmaceutical, Inc. (San Diego, http://www.bdbiosciences.com/index_us.shtml).

In Vivo Cardiomyogenic Differentiation of EMCs

EGFP-labeled EMC tissue graft, made by a novel 3-dimensional cell sheet manipulation, was transplanted into male F344 nude rats (Clea, Tokyo, http://www.clea-japan.com/) (8 weeks of age). EMC100s and EMC214s ($2 \times 10^5/cm^2$) were plated onto fibrin polymer-coated culture dishes. Four days after plating, EMCs were detached as previously described [18], and transplanted onto the surface of the recipient heart (Fig. 5A) [19]. At 2 weeks after transplantation, immunohistochemical analysis was performed. EGFP-labeled EMC tissue graft on the fibrin polymer-coated culture dish did not show cardiomyogenic differentiation in vitro.

MMC Transplantation in Myocardial Infarction Model In Vivo

Recipient male F344 nude rats (Clea) (6 weeks of age) were anesthetized with 2% isoflurane gas. After left thoracotomy, the left ventricle was exposed and left anterior coronary artery was ligated by 6–0 silk suture. The complete occlusion of the coronary artery was confirmed by the cyanotic color and dyskinetic motion of the left ventricular anterior wall. In some rats, we did not ligate the coronary artery (Sham). The chest was closed and animals survived for 2 weeks to create complete myocardial infarction.

Two weeks after the first operation, rats with myocardial infarction were randomized for the control myocardial infarction (MI) group, the MI+BMMSC group, and the MI+MMC group, and were blinded immediately before the cell injection. Echocardiograms were performed on the anesthetized (2% isoflurane) rats. Data were collected three times and averaged. Immediately before transplantation, ~1–2 × 10^6 of EGFP-positive MMC or BMMSC suspension was drawn up into a 50-μl Hamilton syringe (Hamilton Co., Reno, NV, http://www.hamiltoncompany.com/main_usa.asp) with a 31-gauge needle. A 10-μl portion of the cell suspension was injected into the center and margin of the infarcted myocardium (MI+MMC, Fig. 7A). In the control MI group, culture medium or ~1–2 × 10^6 of murine cardiac fibroblast was injected. Immediately before cell transplantation, 2-dimensional and M-mode echocardiographic (8.5 MHz linear transducer, EnVisor C; Phillips Medical System, Andover, MA, http://www.medical.philips.com/index.html) images were obtained to assess left ventricular (LV) end-diastolic dimension and LV end-systolic dimension at the mid-papillary muscle level.

Two weeks after the transplantation, a similar echocardiogram was performed again; then after opening the abdomen, a blood sample was drawn from the abdominal great vein; then the left diaphragm was dissected to insert a 22-gauge manometer line into the left ventricle, which was connected to the transducer (model TP-400T; Nihon Kohden) to monitor left ventricular pressure. The electrocardiogram and measured pressure were digitized by PowerLabo (ADInstruments, Milford, MA, http://www.adinstruments.com) at the sample frequency of 10 KHz and stored in a personal computer (Macintosh iBook G4; Apple, Cupertino, CA, http://www.apple.com).

Tissue samples were obtained by fixing and slicing along the short axis of the left ventricle, for every 1-mm depth of the ventricle. After Masson's trichrome staining, digital images of samples were collected using a light microscope (IX-70; Olympus). The images were digitized and analyzed using an Igor Pro 4 (Wavemetrics Inc.). The pixel area of blue color (fibrosis area) was defined as the infarcted area, and the pixel area of red color was defined as "survived" myocardium. The data on each pixel area from each slice were collated and the percentage fibrosis area was calculated as follows: % Fibrosis = 100 × (Pixel area of blue color)/(Pixel area of blue color and red color).

Statistical Analysis

All data are shown as the mean value ± SE. The difference among mean values was determined with analysis of variance. The posthoc test (Bonferroni) was used when three or more groups were compared. Student's t test was used when two values were compared. Statistical significance was set at $p < .05$.

RESULTS

Cardiomyogenic Transdifferentiation of MMCs

To exclude cell fusion-dependent cardiomyogenesis [20], EGFP-labeled MMCs were cocultured in the same dish with mouse cardiomyocytes, separated by a 40-μm high-density atelocollagen membrane (Fig. 1M). The two cell types were never in direct contact. On day 5 after cocultivation commenced, approximately half of the MMCs were beating strongly in a synchronized manner (supplemental online Video 1). Im-

Downloaded from www.StemCells.com at Keio University Shinanomachi Media Center on August 19, 2008

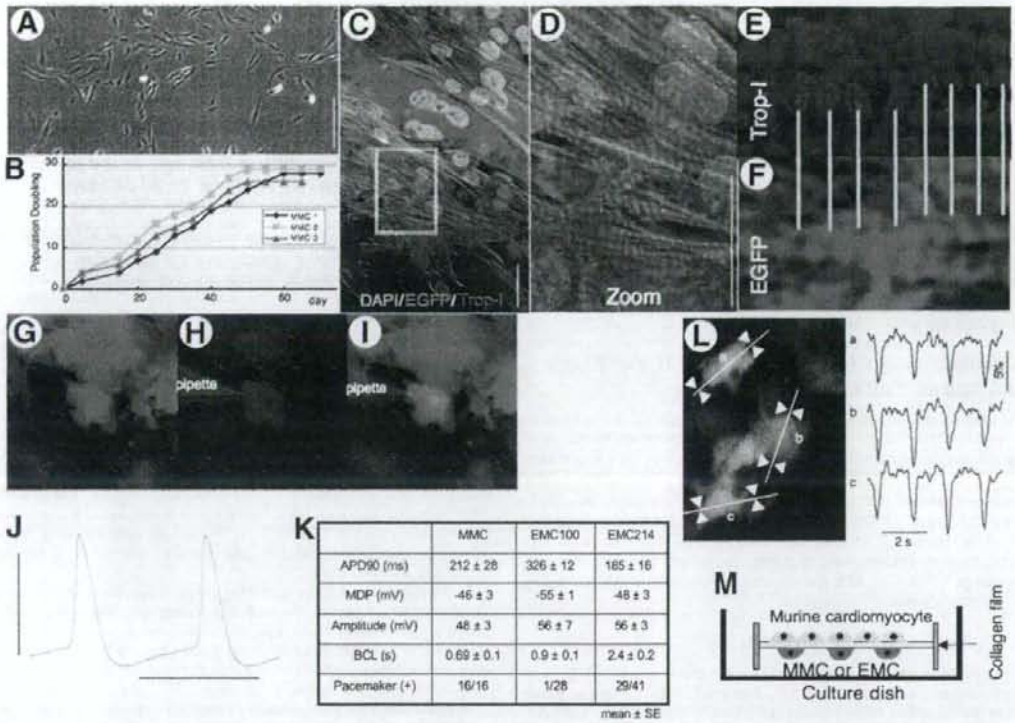

	MMC	EMC100	EMC214
APD90 (ms)	212 ± 28	326 ± 12	185 ± 16
MDP (mV)	-46 ± 3	-55 ± 1	-48 ± 3
Amplitude (mV)	48 ± 3	56 ± 7	56 ± 3
BCL (s)	0.69 ± 0.1	0.9 ± 0.1	2.4 ± 0.2
Pacemaker (+)	16/16	1/28	29/41

mean ± SE

Figure 1. Cardiomyogenic differentiation of menstrual blood-derived mesenchymal cells (MMCs) in vitro. **(A):** Phase-contrast microscopic view of MMC (bar denotes 100 μm), regarded as being PD1, or day 2. **(B):** The representative growth curves of MMCs as a function of time after the culture. The growth curves from all three donors are linear over at least 25 population doublings. **(C–F):** Laser confocal microscopic view of immunocytochemistry of differentiated MMCs with anti-cardiac troponin-I (Trop-I) antibody. Enhanced green fluorescent protein (EGFP)-positive (green) human MMCs expressed Trop-I (red). Scale bar denotes 20 μm. **(D):** Expansion of area within the white box in **(C)**. Clear striation pattern of Trop-I is observed. Trop-I and EGFP images along the yellow line are shown in **(E, F)**. **(E, F):** Trop-I and EGFP staining was observed alternately in striated manner, suggesting Trop-I is expressed in the EGFP-positive cell. **(G–I):** EGFP-labeled MMCs were injected with Alexa 568 solution (red) through a microelectrode to confirm that the recorded signal was obtained from MMCs. **(J):** Representative action potential traces are shown (horizontal line denotes 500 ms). The vertical line denotes 50 mV, and dotted horizontal line denotes 0 mV. **(K):** Action potential parameters. **(L):** A representative still image (left panel) and detected fractional shortening (% FS) along the white line obtained from sites a, b, and c are shown in right panel. **(M):** Experimental schema. Abbreviations: ADP, action potential duration; BCL, basic cycle length; DAPI, 4'-6-diamidino-2-phenylindole; MDP, maximum diastolic potential.

munocytochemistry revealed that the MMCs were stained positive by the anti-cardiac troponin-I antibody (Fig. 1C–1E). Clear striations of red fluorescence of troponin-I in the differentiated MMCs (Fig. 1D, 1E) were observed. Troponin-I and EGFP staining appeared alternately in a striated manner, suggesting troponin-I expressed in the EGFP-positive cell (Fig. 1E, 1F). Clear striations were observed with red fluorescence of α-actinin in the differentiated MMCs (Fig. 2B) and diffuse dot-like staining pattern of connexin 43 around the margin of each EGFP-positive cardiomyocyte (Fig. 2C–2F), suggesting that these human transdifferentiated cardiomyocytes have tight electrical coupling with each other. APs were recorded from spontaneously beating MMCs. The APs obtained from MMCs showed clear cardiomyocyte-specific sustained plateaus and slowly depolarizing resting membrane potentials—so-called "pacemaker potentials" (Fig. 1J, 1K)—and were, therefore, determined to be APs of cardiomyocytes, not of smooth muscle cells, nerve cells, or skeletal muscle cells. The fractional shortening (% FS) of the MMCs was analyzed (Fig. 1L) using a cell edge detection program. The EGFP-positive cells contracted simultaneously within the whole visual field. The % FS was 5.9 ± 0.5% (n = 19).

The percentage of cardiac troponin-I-positive cells was calculated to determine the cardiomyogenic transdifferentiation rate. Whereas MMCs without cocultivation did not show any troponin-I expression (supplemental online Figs. 1A–1D, 2A, 2B), 27%–32% of MMCs became positive for cardiac troponin-I antibody as a result of the cocultivation (Figs. 1C–1F, 4A, supplemental online Fig. 2C, 2D). A cytosine analog, 5-azaC, has a remarkable effect on cell transdifferentiation and has been shown to induce transdifferentiation BMMSCs into cardiomyocytes in mice by nonspecific demethylation of the genome [1]. Cardiomyogenic transdifferentiation was observed in the cocultivated MMCs without any 5-azaC pretreatment, meaning that 5-azaC was not essential for cardiomyogenic transdifferentiation. Nuclear fusion between the cocultivated MMCs and murine cardiomyocytes without separation of the athelocollagen membrane was observed in only 0.16% (3/1846).

Cardiomyogenic Transdifferentiation of EMCs

We hypothesized that the origin of cardiomyogenic cells in the MMCs was the endometrial gland, since MMCs have a high content of detached endometrial glands, whereas circu-

Downloaded from www.StemCells.com at Keio University Shinanomachi Media Center on August 19, 2008

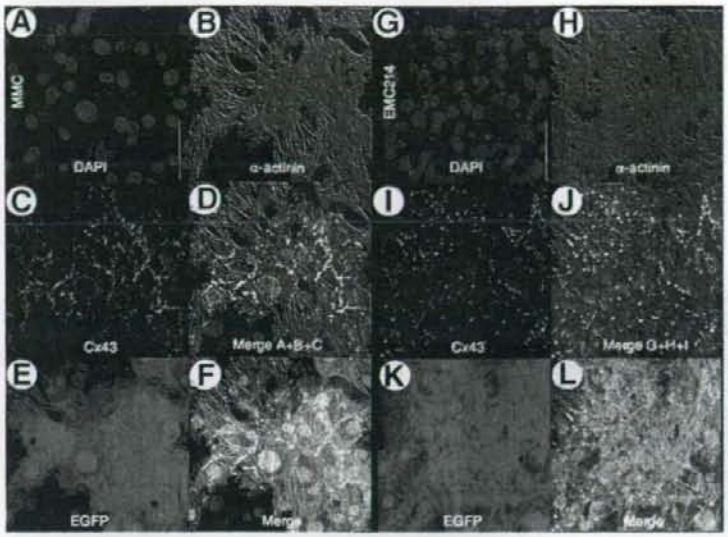

Figure 2. Immunocytochemical analysis of menstrual blood-derived mesenchymal cells (MMCs) and EMC214s stained with anti-sarcomeric α-actinin and connexin 43. **(A–L):** Laser confocal microscopic view of immunocytochemistry of differentiated MMCs and EMC214s with anti-sarcomeric α-actinin (α-actinin) and connexin 43 (Cx43) antibody. **(A–F, G–L):** Enhanced green fluorescent protein (EGFP)-positive **(E, K**; green) human MMCs and EMC214s express α-actinin **(B, H**; red) and Cx43 **(C, I**; cyan). Nuclei are stained with 4′-6-diamidino-2-phenylindole (DAPI) **(A, G**; blue). Clear striation patterns of α-actinin and diffuse Cx43 dot-like staining around the margin of the MMCs and EMC214s were observed. Scale bars in the figure denote 50 μm.

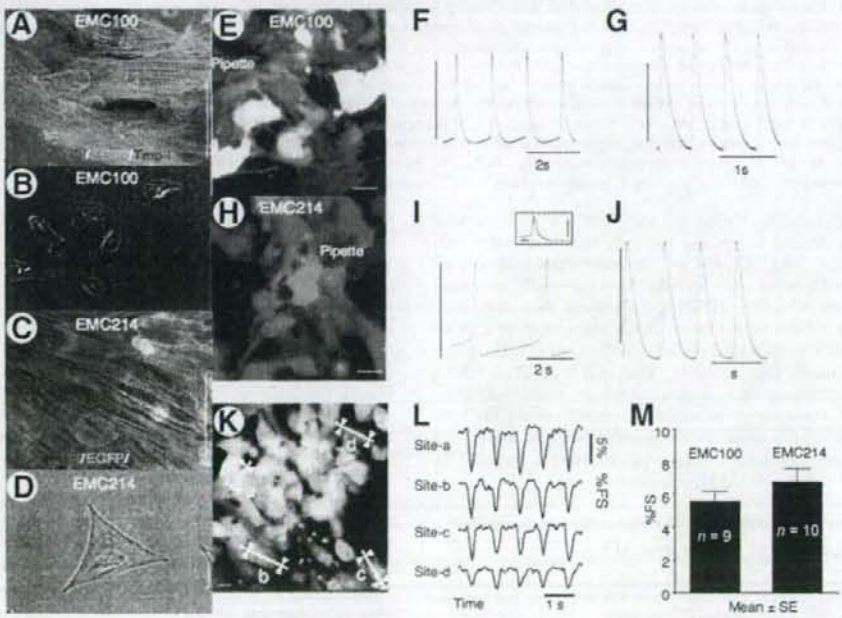

Figure 3. Cardiomyogenic differentiation of endometrial gland-derived mesenchymal cells (EMCs) in vitro. **(A, C):** Immunocytochemistry of differentiated EMC100s **(A)** and EMC214s **(C)** with anti-cardiac troponin-I (Trop-I) antibody. The cells were stained with 4′-6-diamidino-2-phenylindole (DAPI; blue), and anti-cardiac troponin-I antibody (red). Enhanced green fluorescent protein (EGFP)-positive (green) human EMCs expressed Trop-I (red). Please note clear striation staining pattern of Trop-I **(A, C)** in EMCs. Scale bar denotes 20 μm. **(B, D):** Phase-contrast images of EMC100s **(B)** and EMC214s **(D)** before the cardiomyogenic induction. **(E, H):** EGFP-labeled EMC100s and EMC214s (green) were injected with Alexa 568 solution (red) through a microelectrode **(E, H)**, and a recorded signal was obtained from the cells. Representative action potential traces are shown **(F, G**: EMC100; **I, J**: EMC214). Action potential of E is expanded in the inset (the vertical line denotes 100 ms). The vertical line denotes 50 mV and dotted horizontal line denotes 0 mV levels. **(K–M):** A representative still image **(K)** and detected fractional shortening (% FS) along the white line obtained from sites a, b, c, and d in **(L)** are shown in **(M). (M):** The measured % FS was averaged and is shown.

lating blood-derived endothelial progenitor cells [21] or marrow-derived MSCs [2] do not have such high cardiomyogenic differentiation ability. We consequently established a line of EMCs (Fig. 3B, 3D) with a lifespan prolonged by a cell cycle-mediated gene to ensure a supply of cells for analysis. Almost all EMCs beat strongly in a synchronized manner

Downloaded from www.StemCells.com at Keio University Shinanomachi Media Center on August 19, 2008

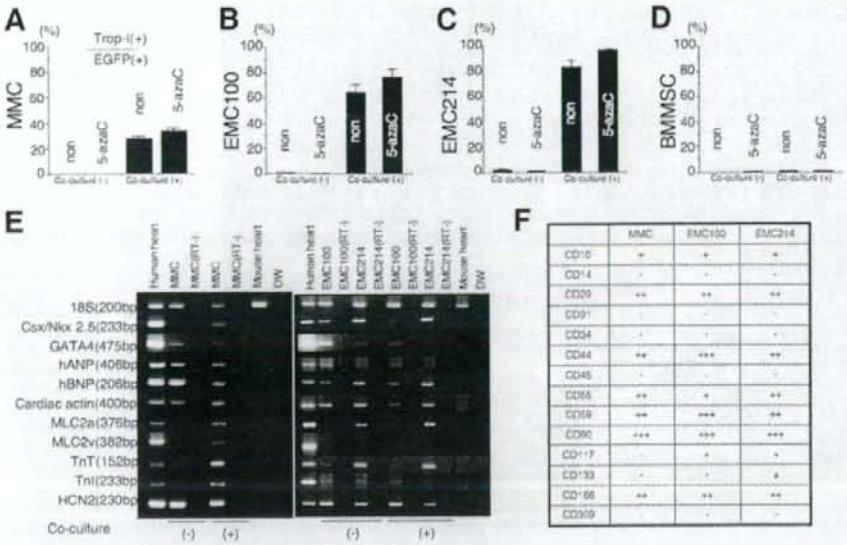

Figure 4. Cardiomyogenic transdifferentiation rates and expression of cardiomyocyte-specific genes and cell surface markers of menstrual blood-derived mesenchymal cells (MMCs) and endometrial gland-derived mesenchymal cells (EMCs). **(A–D):** Cardiomyogenic transdifferentiation rates of MMCs, EMCs, and bone marrow-derived mesenchymal stem cells (BMMSCs). The character in each column denotes pretreatment with 5-azacytidine (5-azaC) or the lack of treatment (non). **(E):** Reverse transcriptase polymerase chain reaction (PCR) was performed with PCR primers with specificity for human genes encoding cardiac proteins but not for the corresponding murine genes (supplemental online Table 1). Human heart and mouse heart cells were used as a positive control and negative control, respectively. Most human cardiac genes were constitutively expressed in the default state of MMCs and EMCs. **(F):** Summary of flow cytometric analysis of MMCs and EMCs with fluorescein isothiocyanate–coupled antibodies against human surface antigens. Abbreviations: DW, distilled water; EGFP, enhanced green fluorescent protein; hANP, human atrial natriuretic peptide; hBNP, human brain natriuretic peptide; HCN2, cyclic nucleotide-gated potassium channel 2; MLC2a, myosin light chain 2a; MLC2V, myosin light chain 2v; TnI, Trop-I, cardiac troponin I; TnT, cardiac troponin T.

(supplemental online Video 1), and 76.4%–96.5% became positive for cardiac troponin-I antibody as a result of cocultivation (Figs. 3A, 3C, 4B, 4C, supplemental online Fig. 2E–2L). EMCs were also positive for sarcomeric α-actinin and connexin 43 (Fig. 2G–2L). APs were recorded from EMCs. The APs obtained from EMCs showed clear cardiomyocyte-specific sustained plateaus and, in some cells, pacemaker potentials (Fig. 3E–3J). The EGFP-positive EMCs contracted simultaneously within the whole visual field (Fig. 3L, 3M). Nuclear fusion between the cocultivated EMC100s or EMC214s and murine cardiomyocytes without separation of the athelocollagen membrane was observed in only 0.57% (6/1058) or 0.28% (5/1758), respectively.

Expression of Cardiomyocyte-Specific Genes and Surface Markers of EMCs and MMCs

The RT-PCR was performed with primers that hybridized with human cardiomyocyte-specific genes but not with the murine orthologs. Differentiated MMCs and EMCs expressed cardiac-specific genes (Fig. 4D). Interestingly, most of the analyzed genes were expressed in the cells before the induction of transdifferentiation by cocultivation.

There is no difference between surface markers of the MMCs and EMCs. Both cells were positive for CD29 (integrin β1), CD59, and negative for CD14, CD34, CD45, CD309 (Flk-1), etc. (Fig. 4E, supplemental online Fig. 3A–3C).

Cardiomyogenic Effects In Vivo

An EGFP-labeled EMC tissue graft made by a novel 3-dimensional cell sheet manipulation [18] was transplanted into male F344 nude rats to ensure in vivo cardiomyogenic transdifferentiation ability. The EGFP-positive cell layer (green) was observed at the epicardial surface of the host heart (Fig. 5B–5D). Whole EMCs throughout the layer expressed a clear striation staining pattern of sarcomeric α-actinin (Fig. 5B–5G), suggesting extremely high cardiomyogenic transdifferentiation ability of EMCs in situ.

MMCs or BMMSCs were transplanted into the nude rats with MI in vivo. Echocardiography showed that the left ventricular fractional shortening (% LVFS) in the MI+MMC group was significantly greater than it in the MI+BMMSC group at 2 weeks after transplantation (Fig. 6A–6I, supplemental online Fig. 4). The MI area was digitized and every 1-mm depth of tissue section stained with Masson's trichrome (Fig. 6J–6O); averaged data are shown in Figure 6P. The MI area was significantly lower in the MI+MMC group than in the MI+BMMSC group. The EGFP-positive mass of MMCs observed in the MI area expressed a clear striation staining pattern of cardiac troponin-I (Fig. 7) and sarcomeric α-actinin (supplemental online Fig. 5), suggesting an extremely high in situ cardiomyogenic transdifferentiation ability of MMCs, which contributed to improvement in cardiac function.

DISCUSSION

Mechanisms of Highly Cardiomyogenic Transdifferentiation Ability of MMCs and EMCs

The gene expression pattern of MMCs and EMCs before cardiomyogenic transdifferentiation is quite different from that of marrow-derived MSCs [2]. GATA-4 expression in the MMCs and EMCs, and Csx/Nkx 2.5 expression in EMCs with the

Downloaded from www.StemCells.com at Keio University Shinanomachi Media Center on August 19, 2008

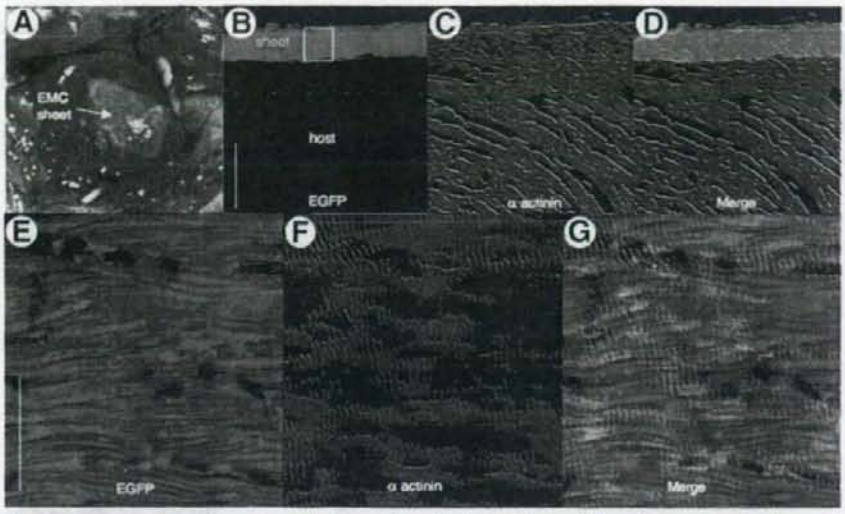

Figure 5. In vivo cardiomyogenesis of endometrium-derived mesenchymal cells (EMCs) in cell sheet tissue graft on host heart. **(A):** Macroscopic view of enhanced green fluorescent protein (EGFP)-labeled EMC tissue graft (sheet) on the epicardial surface of the recipient's heart. **(B–D):** Two weeks after transplantation, immunohistochemistry revealed survival of EMC tissue layer (green) on the recipient heart. Scale bar denotes 100 μm. **(C):** Engrafted EMCs stained positive with anti-sarcomeric α-actinin (red; α-actinin). **(E–G):** The area in the white box in **(B)** is shown in greater detail in **(E–G)**. **(F):** The clear striation pattern of α-actinin staining was observed throughout the entire layer of engrafted EMCs, suggesting extremely high cardiomyogenic potential of EMCs in situ. Scale bar denotes 20 μm.

ability of self-renewal suggest that MMCs and EMCs both have cardiogenic potential and may be termed "cardiac precursor cells" due to their biological features. Cardiac mRNA but not cardiac protein (i.e., troponin-I) was expressed at the default state in the present study, suggesting that both genetic and epigenetic factors may be essential to cause physiologically functioning cardiomyogenic differentiation in MMCs and EMCs. The mechanism of the drastic improvement in the transdifferentiation rate of MMCs and EMCs may be attributable to the default characteristics (expression level of cardiomyocyte-specific mRNA) of MMCs and EMCs in culture compared to marrow-derived MSCs. Highest cardiomyogenic transdifferentiation efficiency was observed in EMC214s (96.5%), EMC100s (76.4%), UCBMSCs (44.9%) [11], MMCs (33.2%), PCPCs (15.1%) [12], and BMMSCs (0.3%, Fig. 4D) [2] in that order. In the practical point of view, EMCs and UCBMSCs are difficult to obtain in enough numbers during the first few passages. MMCs are, therefore, the most suitable cellular source for cardiac stem cell therapy, having a high cardiomyogenic transdifferentiation efficiency. MMCs, EMCs, UCBMSC, and PCPCs are derived from the organ that is related to the pregnancy, therefore the high cardiomyogenic transdifferentiation ability of mesenchymal cells may be caused by a pregnancy-related environmental condition.

Origin of the MMCs and EMCs

Cell surface marker analysis revealed that MMCs are neither encirculating endothelial progenitor cells [22] nor macrophages, but are mesenchymal phenotype cells. We speculated that MMCs may originate in uterine endometrial glands since a lot of detached endometrial glands were observed in menstrual blood and EMCs have the same surface marker as the MMCs, as well as an extremely high cardiomyogenic potential (76.4%–96.5% and 33.2%, respectively). As has been reported, MSCs cannot be detected in circulating blood and all tissues have MSC reservoirs localized in the perivascular niche [23], so EMCs and MMCs do not seem to originate from BMMSCs.

Clinical Contribution

In the present study, MMC transplantation improved impaired cardiac function in vivo. Since MMCs were transplanted at 2 weeks after coronary occlusion, when myocardial necrosis had been completed, the improvement of cardiac function is not due only to transplanted MMC-induced neovascularization [7, 8] or an antiapoptotic [9] effect on infarcted cardiomyocytes. Since they display high cardiomyogenic transdifferentiation ability in vitro and massive cardiomyogenic transdifferentiation in vivo, MMC-derived cardiomyocytes may play a role in the improvement of cardiac function in the present study. Myocardial infarction is known to suppress contraction ability of cardiomyocytes even at normal zone by left ventricular remodeling. Therefore MMC-derived paracrine factors may also play an important role in recovery of % LVFS by prevention of development of LV remodeling.

Neovascularization and the antiapoptotic effect are important for improving cardiac function to some extent. However, the feasible effect is dependent on the number of residual host cardiomyocytes in the infarcted myocardium. To achieve further improvement of cardiac function, a stem cell source that can be expected to exhibit powerful cardiomyogenic transdifferentiation in situ is required. MMCs can be transdifferentiated into cardiomyocytes in situ on the recipient heart, suggesting that they are a promising source for cardiac stem cell-based therapy material, significantly more efficient for cardiomyogenesis than BMMSCs.

MMCs can be readily obtained in a noninvasive manner from young female volunteers, and stored. It should therefore be possible to obtain MMCs of all the HLA types, possibly enabling the establishment of an MMC bank system to facilitate cardiac stem cell-based therapy.

Downloaded from www.StemCells.com at Keio University Shinanomachi Media Center on August 19, 2008

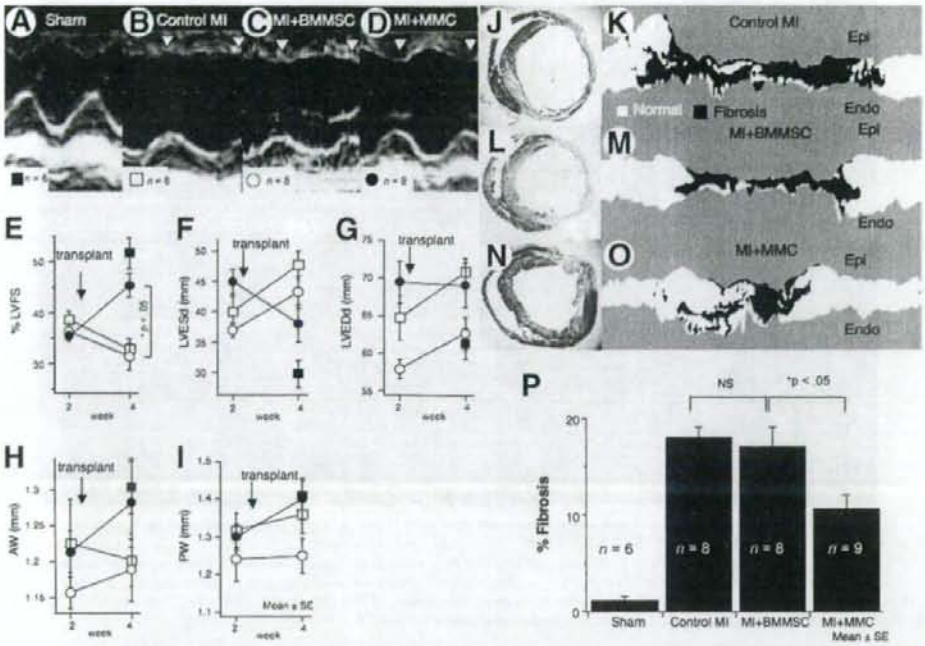

Figure 6. The effect of menstrual blood-derived mesenchymal cell (MMC) transplantation on cardiac function. **(A–D):** Representative M-mode echocardiographic images. The contraction of the left ventricular (LV) anterior wall was improved by transplantation of MMCs (white arrows). The symbol of and number in each group is depicted at the bottom left of each image. **(E–I):** Measured LV parameters are averaged and shown at 2 weeks and 4 weeks after the myocardial infarction (MI). The significant improvement of **(F)** LV end-systolic diameter (LVESd) and **(E)** % fractional shortening (% LVFS) were observed. The diameter of **(H)** anterior left ventricular wall thickness (AW), and **(I)** posterior left ventricular wall thickness (PW). There is no statistical significance. **(J–O):** Representative Masson's trichrome stain images **(J, L, N)** and digitized images **(K, M, O)** of control MI group, MI+bone marrow-derived mesenchymal stem cell (BMMSC), and MI+MMC group are shown. **(P):** The calculated % fibrosis areas are summed and averaged. The MMC transplantation showed significant reduction of % fibrosis area. Abbreviations: Endo, endocardium; Epi, epicardium; NS, not significant.

Role of Established Cardiomyogenic EMC Cell Line for Determining Cardiomyogenic Factors

Several stem cell types are used for clinical patients. Of these, MSCs are reported to show cardiomyogenesis in vitro. Thus, the analysis of key mechanisms for cardiomyogenic differentiation in the human mesenchymal cell is extremely important in order to expand the efficacy of current cardiac stem cell therapy. However, it is very difficult to specify the key factor of cardiomyogenesis by in vivo experiment only. Establishment of EMCs and an in vitro cardiomyogenic differentiation assay system are essential. Stable and high cardiomyogenic transdifferentiation ability in our established system enables us to observe, with wide dynamic range, the effects of treatment for cardiomyogenesis. Moreover, the primary culture condition of murine cardiomyocytes usually fluctuates due to variations in environments, the skill of individual researchers, and institutional differences in isolation protocols. Our established EMCs may provide a good positive control for a cardiomyogenic assay system in vitro to check whether the feeder cell condition is suitable for cardiomyogenic assay. When feeder conditions are suitable, we can survey for possible cardiomyogenic assistant factors or appropriate culture conditions for human BMMSCs by applying various agents or modifying culture conditions systematically. Thus, by using our EMCs and cocultivation system, we may be able to expand the cardiomyogenic differentiation potential of marrow-derived MSCs. Consequently, we may be able to increase the efficacy of cardiac stem cell-based therapy dramatically.

Neither passive stretching of EMCs nor an application of the supernatant of murine cardiomyocyte culture medium to the EMCs alone caused cardiomyocyte differentiation. Taking these findings into account, the multiple environmental factors, including mechanical stretching and/or feeder cardiomyocyte-derived humoral factors, seem to contribute to cardiomyogenic transdifferentiation in human mesenchymal cells. Further experiments should be done.

Study Limitations

Cell fusion between the human cells (MMCs or EMCs) might be a major cause of EGFP-positive cardiomyocytes in the present study. However, EGFP-positive cardiomyocytes could be observed, even when human cells and murine cardiomyocytes were cocultured separately by the athelocollagen membrane that is permeable for only small molecules (less than 5,000 MW)—thus allowing no possible penetration of cells or organelles through the membrane (supplemental online Fig. 6). Furthermore, even if the cells were cocultured without the athelocollagen membrane, nuclear fusion between EMC100s, EMC214s, or MMCs and fetal murine cardiomyocytes was less than 1% in the present study. Moreover, transdifferentiated EMCs at the external layer of the cell sheet graft on the epicardial surface did not directly contact the host cardiomyocytes (Fig. 5). Taking these results

Downloaded from www.StemCells.com at Keio University Shinanomachi Media Center on August 19, 2008

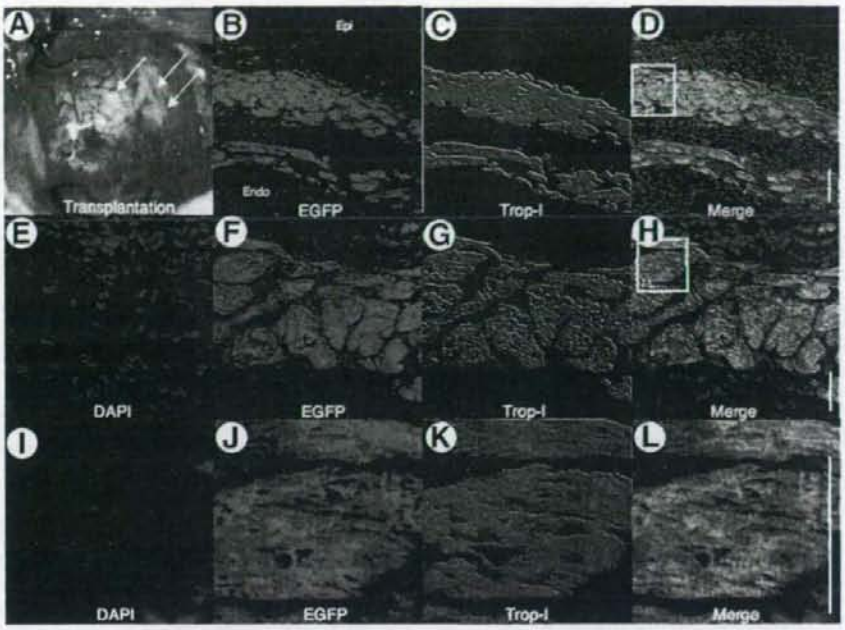

Figure 7. Cardiomyogenesis of engrafted menstrual blood-derived mesenchymal cells (MMCs) in vivo. **(A):** Macroscopic view of the recipient's heart immediately after enhanced green fluorescent protein (EGFP)-labeled MMC transplantation (white arrows) into the myocardial infarction area of the recipient's heart. **(B–L):** Two weeks after transplantation, immunohistochemistry revealed survival of the MMC tissue layer (green) on the treated heart. **(B–D):** Engrafted MMCs stained positive with anti-cardiac troponin-I (red; Trop-1). Scale bar denotes 100 μm. **(E–H, I–L):** The area in the white box in **(D)** was observed in higher resolution **(E–H)** and the white box in **(H)** was also observed in higher resolution **(I–L)**. **(K):** The clear striation pattern of Trop-1 staining was observed throughout the whole layer of engrafted MMCs, suggesting extremely high cardiomyogenic potential of MMCs in situ. Scale bar denotes 20 μm. Abbreviations: DAPI, 4′-6-diamidino-2-phenylindole; Endo, endocardium; Epi, epicardium.

into account, we concluded that the cell fusion did not play a major role in the observed significant cardiomyogenic potential of MMCs and EMCs in the present study.

Infarcted heart tissue may increase auto-fluorescence in some fixative conditions and such auto-fluorescence of host cardiomyocytes might be confused as EGFP-positive like cells. However, autofluorescence of the host myocardium adjacent to the infarcted area was not significant in our present condition (Figs. 5B, 6B, supplemental online Fig. 5B, 5F). Therefore, EGFP-positive tissue in the present study can be defined as of human cell origin and easily distinguished from the host heart by the EGFP fluorescent intensity.

The transfection of the cell cycle-mediated gene may increase cardiomyogenic differentiation to some extent. However, our previous study in human BMMSCs, [2] with the same combination of cell cycle-mediated gene transfection, did not show any increase in efficiency. Furthermore, non-gene-transfected MMCs have an extremely high cardiomyogenic efficiency compared to gene-transfected BMMSCs. Taking these results into account, we concluded that transfection of those genes does not play an essential role in causing such high cardiomyogenic differentiation efficiency in EMCs.

In comparison to previous papers, there was no observable effect of BMMSC transplantation on cardiac function in the present study. This discrepancy may be caused by different experimental conditions, that is, species difference between BMMSCs and the host animal [24], transplantation at acute myocardial infarction [25–27], and usage of immunosuppressive agents, etc [24–27].

In the present study, we did not use a pressure-tipped catheter, therefore the LV dp/dt value may be underestimated.

Summary

MMC transplantation decreased fibrosis area and restored the LV systolic function in the MI-model in vivo. Engrafted MMC transdifferentiated into cardiomyocyte within MI area. MMC can be a major cell source for stem cell therapy to achieve cardiomyogenesis.

Acknowledgments

The research of N.H. and N.N. was partially supported by a grant from the Ministry of Education, Science and Culture, Japan. A part of this work was undertaken at the Keio Integrated Medical Research Center. We thank M. Uchiyama, A. Furuta, K. Hayakawa, and K. Okamoto for help during the experiments. N.H. and N.N. contributed equally to this work. A part of this work was reported at the annual meeting of the American College of Cardiology 2005, 2006, and 2007.

Disclosure of Potential Conflicts of Interest

The authors indicate no potential conflicts of interest.

Downloaded from www.StemCells.com at Keio University Shinanomachi Media Center on August 19, 2008.

REFERENCES

1 Makino S, Fukuda K, Miyoshi S et al. Cardiomyocytes can be generated from marrow stromal cells in vitro. J Clin Invest 1999;103:697–705.
2 Takeda Y, Mori T, Imabayashi H et al. Can the life span of human marrow stromal cells be prolonged by bmi-1, E6, E7, and/or telomerase without affecting cardiomyogenic differentiation? J Gene Med 2004;6: 833–845.
3 Chen SL, Fang WW, Ye F et al. Effect on left ventricular function of intracoronary transplantation of autologous bone marrow mesenchymal stem cell in patients with acute myocardial infarction. Am J Cardiol 2004;94:92–95.
4 Orlic D, Kajstura J, Chimenti S et al. Bone marrow cells regenerate infarcted myocardium. Nature 2001;410:701–705.
5 Wang JS, Shum-Tim D, Galipeau J et al. Marrow stromal cells for cellular cardiomyoplasty: Feasibility and potential clinical advantages. J Thorac Cardiovasc Surg 2000;120:999–1005.
6 Shake JG, Gruber PJ, Baumgartner WA et al. Mesenchymal stem cell implantation in a swine myocardial infarct model: Engraftment and functional effects. Ann Thorac Surg 2002;73:1919–1926.
7 Gojo S, Gojo N, Takeda Y et al. In vivo cardiovasculogenesis by direct injection of isolated adult mesenchymal stem cells. Exp Cell Res 2003; 288:51–59.
8 Tang YL, Zhao Q, Zhang YC et al. Autologous mesenchymal stem cell transplantation induce VEGF and neovascularization in ischemic myocardium. Regul Pept 2004;117:3–10.
9 Gnecchi M, He H, Liang O et al. Paracrine action accounts for marked protection of ischemic heart by Akt-modified mesenchymal stem cells. Nat Med 2005;11:367–368.
10 Kocher AA, Schuster MD, Szabolcs MJ et al. Neovascularization of ischemic myocardium by human bone-marrow-derived angioblasts prevents cardiomyocyte apoptosis, reduces remodeling and improves cardiac function. Nat Med 2001;7:430–436.
11 Nishiyama N, Miyoshi S, Hida N et al. The significant cardiomyogenic potential of human umbilical cord blood-derived mesenchymal stem cells in vitro. STEM CELLS 2007;25:2017–2024.
12 Okamoto K, Miyoshi S, Toyoda M et al. 'Working' cardiomyocytes exhibiting plateau action potentials from human placenta-derived extraembryonic mesodermal cells. Exp Cell Res 2007;313:2550–2562.
13 Terai M, Uyama T, Sugiki T et al. Immortalization of human fetal cells: the life span of umbilical cord blood-derived cells can be prolonged without manipulating p16INK4a/RB braking pathway. Mol Biol Cell 2005;16:1491–1499.
14 Takeuchi M, Takeuchi K, Kohara A et al. Chromosomal instability in human mesenchymal stem cells immortalized with human papilloma virus E6, E7, and Htert genes. In Vitro Cell Dev Biol Anim 2007;43: 129–138.
15 Schwab KE, Gargett CE. Co-expression of two perivascular cell markers isolates mesenchymal stem-like cells from human endometrium. Hum Reprod 2007;22:2903–2911.
16 Meng X, Ichim TE, Zhong J et al. Endometrial regenerative cells: A novel stem cell population. J Transl Med 2007;5:57–66.
17 Kyo S, Nakamura M, Kiyono T et al. Successful immortalization of endometrial glandular cells with normal structural and functional characteristics. Am J Pathol 2003;163:2259–2269.
18 Itabashi Y, Miyoshi S, Kawaguchi H et al. A new method for manufacturing cardiac cell sheets using fibrin-coated dishes and its electrophysiological studies by optical mapping. Artificial Organs 2004;29:95–103.
19 Furuta A, Miyoshi S, Itabashi Y et al. Pulsatile cardiac tissue grafts using a novel three-dimensional cell sheet manipulation technique functionally integrates with the host heart, in vivo. Circ Res 2006;98:705–712.
20 Iijima Y, Nagai T, Mizukami M et al. Beating is necessary for transdifferentiation of skeletal muscle-derived cells into cardiomyocytes. FASEB J 2003;17:1361–1363.
21 Koyanagi M, Urbich C, Chavakis E et al. Differentiation of circulating endothelial progenitor cells to a cardiomyogenic phenotype depends on E-cadherin. FEBS Lett 2005;579:6060–6066.
22 Asahara T, Murohara T, Sullivan A et al. Isolation of putative progenitor endothelial cells for angiogenesis. Science 1997;275:964–967.
23 da Silva Meirelles L, Chagastelles PC, Nardi NB. Mesenchymal stem cells reside in virtually all post-natal organs and tissues. J Cell Sci 2006;119:2204–2213.
24 Wang JA, Fan YQ, Li CL et al. Human bone marrow-derived mesenchymal stem cells transplanted into damaged rabbit heart to improve heart function. J Zhejiang Univ Sci B 2005;6:242–248.
25 Zhang S, Ge J, Sun A et al. Comparison of various kinds of bone marrow stem cells for the repair of infarcted myocardium: Single clonally purified non-hematopoietic mesenchymal stem cells serve as a superior source. J Cell Biochem 2006;99:1132–1147.
26 Grauss RW, Winter EM, van Tuyn J et al. Mesenchymal stem cells from ischemic heart disease patients improve left ventricular function after acute myocardial infarction. Am J Physiol Heart Circ Physiol 2007;293: H2438–H2447.
27 Hou M, Yang KM, Zhang H et al. Transplantation of mesenchymal stem cells from human bone marrow improves damaged heart function in rats. Int J Cardiol 2007;115:220–228.

See www.StemCells.com for supplemental material available online.

Downloaded from www.StemCells.com at Keio University Shinanomachi Media Center on August 19, 2008

Gremlin Enhances the Determined Path to Cardiomyogenesis

Daisuke Kami[1,3], Ichiro Shiojima[4], Hatsune Makino[1], Kenji Matsumoto[2], Yoriko Takahashi[1], Ryuga Ishii[1], Atsuhiko T. Naito[4], Masashi Toyoda[1], Hirohisa Saito[2], Masatoshi Watanabe[3], Issei Komuro[4], Akihiro Umezawa[1]*

1 Department of Reproductive Biology, National Institute for Child Health and Development, Tokyo, Japan, 2 Department of Allergy and Immunology, National Institute for Child Health and Development, Tokyo, Japan, 3 Laboratory for Medical Engineering, Division of Materials Science and Chemical Engineering, Graduate School of Engineering, Yokohama National University, Yokohama, Japan, 4 Department of Cardiovascular Science and Medicine, Chiba University Graduate School of Medicine, Chiba, Japan

Abstract

Background: The critical event in heart formation is commitment of mesodermal cells to a cardiomyogenic fate, and cardiac fate determination is regulated by a series of cytokines. Bone morphogenetic proteins (BMPs) and fibroblast growth factors have been shown to be involved in this process, however additional factors needs to be identified for the fate determination, especially at the early stage of cardiomyogenic development.

Methodology/Principal Findings: Global gene expression analysis using a series of human cells with a cardiomyogenic potential suggested *Gremlin* (*Grem1*) is a candidate gene responsible for *in vitro* cardiomyogenic differentiation. Grem1, a known BMP antagonist, enhanced DMSO-induced cardiomyogenesis of P19CL6 embryonal carcinoma cells (CL6 cells) 10–35 fold in an area of beating differentiated cardiomyocytes. The Grem1 action was most effective at the early differentiation stage when CL6 cells were destined to cardiomyogenesis, and was mediated through inhibition of BMP2. Furthermore, BMP2 inhibited Wnt/β-catenin signaling that promoted CL6 cardiomyogenesis.

Conclusions/Significance: Grem1 enhances the determined path to cardiomyogenesis in a stage-specific manner, and inhibition of the BMP signaling pathway is involved in initial determination of Grem1-promoted cardiomyogenesis. Our results shed new light on renewal of the cardiovascular system using Grem1 in human.

Citation: Kami D, Shiojima I, Makino H, Matsumoto K, Takahashi Y, et al. (2008) Gremlin Enhances the Determined Path to Cardiomyogenesis. PLoS ONE 3(6): e2407. doi:10.1371/journal.pone.0002407

Editor: Hernan Lopez-Schier, Centre de Regulacio Genomica, Spain

Received January 15, 2008; **Accepted** May 5, 2008; **Published** June 11, 2008

Copyright: © 2008 Kami et al. This is an open-access article distributed under the terms of the Creative Commons Attribution License, which permits unrestricted use, distribution, and reproduction in any medium, provided the original author and source are credited.

Funding: This study was supported by a grant from the Ministry of Education, Culture, Sports, Science and Technology (MEXT) of Japan and Health and Labor Sciences Research Grants; by a Research grant on Health Science Focusing on Drug Innovation from the Japan Health Science Foundation; by the Program for Promotion of Fundamental Studies in Health Science of the Pharmaceuticals and Medical Devices Agency; by a grant from the Terumo Life Science Foundation; by a Research Grant for Cardiovascular Disease from the Ministry of Health, Labor and Welfare (MHLW); and by a Grant for Child Health and Development from the MHLW.

Competing Interests: The authors have declared that no competing interests exist.

* E-mail: umezawa@1985.jukuin.keio.ac.jp

Introduction

The critical event in heart formation is commitment of mesodermal cells to a cardiomyogenic fate and their migration into anterolateral regions of the embryo during late gastrulation. In this process, morphogenic movements and cardiac fate determination are regulated by cytokines such as bone morphogenetic proteins (BMPs) [1–3], and fibroblast growth factors (FGFs) [4–7]. These secreted proteins from neighboring endoderm, ectoderm, and the mesoderm itself, play important roles in induction of cardiac transcription factors [8] and differentiation of cardiomyocytes in amphibians [9] and avians [4]. Cardiomyogenic signals, such as BMPs and FGFs, indeed activate expression of cardiac specific transcriptional factors (Csx/Nkx2.5, Gata4, Mef2c), and these transcriptional factors activate expression of circulating hormones (atrial natriuretic peptide (ANP), brain natriuretic peptide (BNP)), and cardiac specific proteins (myosin heavy chain (MyHC), myosin light chain (MyLC)). Wnt family proteins, cysteine-rich, and secreted glycoproteins, have also been implicated in embryonic development [10,11], and cardiomyogenesis [12,13]. In *Drosophila*, '*wingless*', a homologue of vertebrate Wnt is involved in expression of '*tinman*', a *Drosophila* homologue of Csx/Nkx2.5, through '*armadillo*', a *Drosophila* ortholog of β-catenin, and drives heart development [14]. In vertebrates, however, Wnt1/3a, which activates the canonical Wnt/β-catenin signaling pathway leading to stabilization of β-catenin as a downstream molecule through inactivation of glycogen synthase kinase-3β, inhibits cardiomyocytic differentiation from cardiac mesoderm [15–18]. Wnt11 promotes cardiac differentiation via the non-canonical pathway in *Xenopus* [12] and murine embryonic cell lines [19]. The secretion of Wnt inhibitors such as 'Cerberus', 'Dickkopf' and 'Crescent' by the anterior endoderm prevents Wnt3a secreted by the neural tube from inhibiting heart formation [15–17].

In this study, we performed GeneChip analysis to identify multiple extracellular determinants, such as cytokines, cell

membrane-bound molecules and matrix responsible for cardiomyogenic differentiation, and evaluated the statistical significance of differential gene expression by NIA array analysis (http://lgsun.grc.nia.nih.gov/ANOVA/) [20], a web-based tool for microarray data analysis. We found that Grem1 enhances the determined path to cardiomyogenesis in a stage-specific manner, and that inhibition of the BMP signaling pathway is, at least in part, involved in initial determination of Grem1-promoted cardiomyogenesis.

Results

GeneChip and statistical analysis

To identify cytokines and transcription factors responsible for cardiomyogenic differentiation, 69 human cells were analyzed, depending on gene expression levels, by GeneSpringGX software, and clustered into 30 groups (Fig. 1A, Table 1). Among the 30 groups, 21 groups included cells with a cardiomyogenic potential (Fig. 1B: red numbers). To identify genes specific for these groups, hierarchical clustering was employed, using the average distance method. Genes with the lowest average expression E(G1) within the cluster that can differentiate into cardiomyocytes and genes with the highest average expression E(G2) outside the cluster were identified, as previously described [20–22]. Genes which have E(G1)>E(G2) were estimated, using the False Discovery Rate (FDR<0.05). Grem1 was nominated as a cluster-specific cardiomyocyte-promoting gene in cells that could differentiate into cardiomyocytes following NIA array analysis (Fig. 1B). The gene expression profile reported in this paper has been deposited in the Gene Expression Omnibus (GEO) database (http://www.ncbi.nlm.nih.gov/geo: accession no. GSE8481, GSM41342-GSM41344, and GSM201137- GSM201145).

Cardiomyogenic differentiation of CL6 cells with Grem1 and DMSO

To investigate cardiomyogenic activity of Grem1, P19CL6 embryonal carcinoma cells (CL6 cells) were used for assessment of *in vitro* cardiomyogenic differentiation, since CL6 cells are reproducibly and stably induced into beating cardiomyocytes by DMSO (Fig. 2Aa) [23]. CL6 cells did not differentiate following exposure to Grem1 alone at concentrations of 63 or 125 ng/ml for 14 days (Fig. 2B). However, Grem1 dramatically promotes DMSO-induced cardiomyogenic differentiation at a concentration of 63 and 125 ng/ml; Grem1 (125 ng/ml) especially increased DMSO-induced cardiomyogenic differentiation of CL6 cells as assessed by beating area (Fig. 2Ab and B) (Movie S1 and S2, http://1954.jukuin.keio.ac.jp/umezawa/kami/index.html).

RT-PCR of differentiated or undifferentiated CL6 cells

To investigate gene expression as well as morphological analysis, i.e. beating, during cardiomyogenic differentiation, RT-PCR analysis was performed to detect expression of cardiomyocyte-specific/associate transcription factors, and structural genes (Fig. 2C). Genes encoding *Csx/Nkx2.5*, *Gata4*, *Hand2*, *Mef2c*, *ANP*, *BNP*, *MyLC-2a*, *MyLC-2v*, and *β-MyHC* were up-regulated during cardiomyogenic differentiation of CL6 cells treated with Grem1 and DMSO (Fig. 2C: lanes 6, 7 versus lane 3). Triplicate independent experiments confirmed the concentration-dependent Grem1 action on cardiomyogenic differentiation. The cardiomyocyte-specific genes (*Csx/Nkx2.5*, *Gata4*, *MyLC-2a*, *MyLC-2v*) expression level of CL6 cells treated with DMSO and Grem1 (63 and 125 ng/ml) were also the same as or higher than that of DMSO-induced CL6 cells by semi-quantitative RT-PCR (Figure S1).

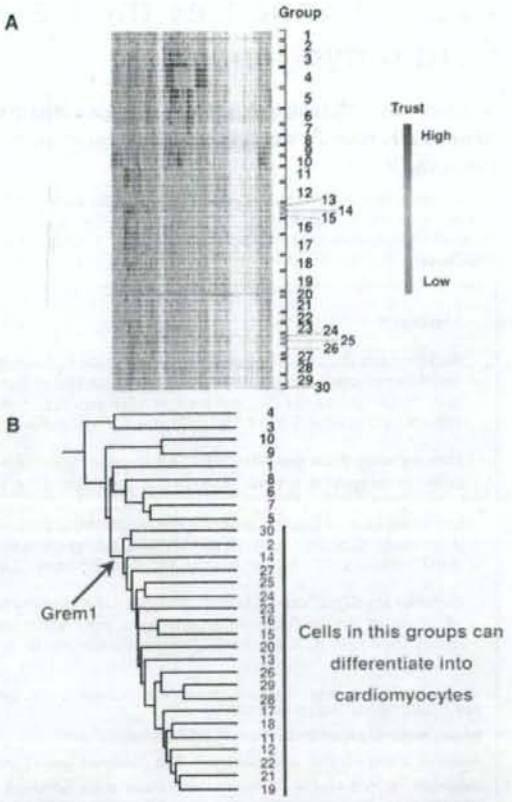

Figure 1. Hierarchical clustering analysis on cultured human cells. (A) Hierarchical clustering analyzed by GeneSpring. Based on gene expression pattern, 69 human cells were clustered into 30 sub-groups. The raw data from the GeneChip analysis are available at the GEO database with accession number GSE8481, GSM41342- GSM41344, and GSM201137- GSM201145. **(B)** Hierarchical clustering analysis was performed by NIA array (http://lgsun.grc.nia.nih.gov/ANOVA/), using averaged values of 30 sub-groups. Among the 30 groups, 21 groups included cells with a cardiomyogenic potential. To identify genes specific for these groups, hierarchical clustering was employed. *Grem1* was nominated as a cluster-specific cardiomyocyte-promoting gene in cells that could differentiate into cardiomyocytes.
doi:10.1371/journal.pone.0002407.g001

Immunocytochemistry of differentiated or undifferentiated CL6 cells

To examine CL6 cells for expression of cardiomyocytic protein, immunocytochemical analysis was performed. CL6 treated with Grem1 (125 ng/ml) and DMSO exhibited clear striation with immunostain using anti-cTnT or anti-α-actinin (Fig. 2Da and b). The MF20- and cTnT-positive cells after exposure to Grem1 and DMSO formed clusters (Fig. 2Ea), compared with the cells after exposure to DMSO alone (Fig. 2Eb). CL6 cells treated with Grem1 alone were negative for MF20 and cTnT, but became positive for both markers following exposure to Grem1 (63 and 125 ng/ml) and DMSO (Fig. 2F). The beating area (Fig. 2B) showed a tendency similar to the MF20- and cTnT-positive area (Fig. 2F), thus there were positive correlations between them.

Table 1. 69 human cells clustered into 30 groups

Group		Title	Description	GSM
1	Normal epithelial cell,primary	NHEK-Neo1	Normal epidermal keratinocyte, neonate, primary	GSM210361
		NHBE-1	Normal bronchial epithelial cell, primary	GSM210362
2	Pulmonary epithelial cell line	A549	Pulmonary epithelial cell line	GSM210363
		BEAS-2B control (6hr)	Bronchial epithelial cell line	GSM210364
3	Lymphocyte	RPMI8226control (6hr)	B cell line	GSM210365
		Raji-1	B cell line	GSM210366
		NK92	NK cell line	GSM210367
4	Myelomonocytic leukemia	U937c	U937 control	GSM210368
		U937h	U937+HRF	GSM210369
		U937ha	U937+HRF+antibody	GSM210370
		U937a	U937+antibody	GSM210371
5	Embryonal carcinoma, cancer	NCR-G3	Embryonal carcinoma, NCR-G3, non-adherent	GSM201141
		NCR-G2NAd	Embryonal carcinoma, NCR-G2, non-adherent	GSM210373
		NCR-G4Ad	Embryonal carcinoma, NCR-G4, adherent	GSM201142
		NCR-G3Ad	Embryonal carcinoma, NCR-G3, adherent	GSM210375
6	ES cell	H1_P43	Undifferentiated hES	GSM41342
		H1-P46	Undifferentiated hES	GSM41343
		H1-P41	Undifferentiated hES	GSM41344
7	Embryonal carcinoma, cancer	NCR-G2Ad	Embryonal carcinoma, NCR-G2, adherent	GSM201140
		NCR-G1	Embryonal carcinoma, NCR-G3, non-adherent	GSM201139
8	Ewing, cancer	NCR-EW2	Ewing, cancer	GSM210378
		NCR-EW3	Ewing, ETV4, cancer	GSM210379
9	Ewing, cancer	GST6	Ewing, POUSF1, cancer	GSM201137
		GST6-extra	Ewing, POUSF1, cancer	GSM210381
10	Ewing, cancer	GST6-5az	Ewing, POUSF1, 5azaC, cancer	GSM201138
		GST6-5az-extra	Ewing, POUSF1, 5azaC, cancer	GSM210383
11	Bone marrow cell, primary	H4-1	Bone marrow cell, primary	GSM201143
		UBT5	Bmi-1, hTERT, bone marrow cell	GSM210385
		UBET7	Bmi-1, E6, hTERT, bone marrow cell	GSM210386
12	Ligament-derived cells	#10	Ligament, primary	GSM210387
	Marrow stromal cells	H10-2Vec	Vector, bone marrow cell	GSM210388
		H10-2TERT	hTERT, bone marrow cell	GSM210389
		H10-2Bmi1	Bmi-1, bone marrow cell	GSM210390
13	Placenta, primary	PL90	Placenta, primary	GSM210391
14	De-differentiated chondrocyte	TdHC1	E6, E7, hTERT, de-differentiated chondrocyte	GSM210392
15	Neural differentiated marrow stromal cell	UET13 Neural differentiation	E7, hTERT, neural differentiation, bone marrow cell	GSM210393
16	Neural differentiated marrow stromal cell	UET13 Neural differentiation1	E7, hTERT, neural differentiation, bone marrow cell	GSM210394
		UET13 Neural differentiation4	E7, hTERT, neural differentiation, bone marrow cell	GSM210395
		UET13 Neural differentiation5	E7, hTERT, neural differentiation, bone marrow cell	GSM210396
17	Cord blood-derived cells	UET13	E7, hTERT, bone marrow cell	GSM210397
		UCB408	Cord blood, primary	GSM210398
		UCB408E6E7-31	E6, E7, umbilical cord blood	GSM210399
	Adipocyte cell, primary	HAdPC1(5/21)	HAdpc1E6E7TERT28	GSM210400
18	Marrow mesenchymal cell, primary	UEET12	E6, E7, hTERT, bone marrow cell	GSM210401
		UEE16	E6, E7, bone marrow cell	GSM210402
		EPC hTERT+1	E6, E7, hTERT, endometrial cell	GSM201144
19	Cord blood, primary	UCB302	Cord blood, primary	GSM210382
		UCB302-D7	Cord blood, primary	GSM210405
		UCB302TERT	hTERT, cord blood	GSM210406
		UET9	E7, hTERT, bone marrow cell	GSM210407

Table 1. cont.

Group		Title	Description	GSM
20	Cord blood, primary	UCB408E7-32	E7, hTERT, cord blood	GSM210408
21	Fetal fibroblast, primary	HFDPC cont.	Normal follicular dermal papillar cell, primary	GSM210409
		PL112	Placenta, primary	GSM210410
		HF7-3	Fetal fibroblast, primary	GSM210411
22	Bone marrow cell, primary	3F0664	Bone marrow cell (commercial item), primary	GSM201145
		BM-MSC	Bone marrow-derived mesenchymal stem cells	GSM38627
23	ES cell-derived mesenchymal cell	H1 clone 2	ES cell-derived mesenchymal precursor	GSM38628
		H9 clone 1	ES cell-derived mesenchymal precursor	GSM38629
24	Endometrial cell	EPC100	E6, E7, hTERT, endometrial cell	GSM210413
25	Bone marrow cell, primary	Yub10F	Bone marrow cell, primary	GSM210414
26	Endometrial cell	EPC hTERT+2	E6, E7, hTERT, endometrial cell	GSM210415
		EPC Control	E6, E7, hTERT, endometrial cell	GSM210416
27	Endometrial cell	EPC214	E6, E7, hTERT, endometrial cell	GSM210417
28	Menstruation blood-derived mesenchymal cell, primary	#E4	Menstruation blood, primary	GSM210418
		#E4HRF	Menstruation blood, HRF treatment, primary	GSM210419
		#E5HRF	Menstruation blood, HRF treatment, primary	GSM210420
29	Menstruation blood-derived mesenchymal cell, primary	#E6	Menstruation blood, primary	GSM210421
		#E6HRF	Menstruation blood, HRF treatment, primary	GSM210422
30	Menstruation blood-derived mesenchymal cell, primary	#E5	Menstruation blood, primary	GSM210423

doi:10.1371/journal.pone.0002407.t001

Grem1 and DMSO were most effective at the early stage (days 1–3) of CL6 differentiation

To determine if Grem1 (125 ng/ml) functions during the early or the late stage of differentiation, CL6 cells were treated with Grem1 for different time periods (Fig. 3A). Grem1 and DMSO were most effective on CL6 differentiation at 1–3 days (Fig. 3B, C) as assessed by percentages of MF20-positive area and beating area. Since Grem1 inhibits BMPs through direct binding [24], we hypothesized that BMP signaling is inhibitory to CL6 cardiomyogenesis during days 1–3. To confirm this hypothesis, RT-PCR analysis was performed to determine expression of the early mesodermal marker (*BrachyuryT* and *Tbx6*), cardiomyocyte-specific transcription factors (*Csx/Nkx2.5*), structural genes (*β-MyHC*), and *Gapdh* (Fig. 4A). DMSO induced the *BrachyuryT* and *Tbx6* genes, and their expressions peaked at 3 days and then decreased; BMP2 down-regulated expression of these genes at 3–7 days. The *Csx/Nkx2.5* and *β-MyHC* genes started to be expressed at days 3 and 5, respectively, and their expression increased up to 14 days, at which time the timeframe analysis was terminated. BMP2 clearly inhibited expression of the *Csx/Nkx2.5* and *β-MyHC* genes (Fig. 4A, lanes 1–7 versus lanes 8–14).

To examine cardiomyogenic differentiation, immunocytochemical analysis was performed on CL6 cells treated with the inducers. CL6 cells treated with DMSO and BMP2 for the first 3 days were negative for sarcomeric myosin (MF20) at 14 days, but became positive for sarcomeric myosin, following exposure to DMSO alone during days 1–3 (Fig. 4B). To determine if DMSO induces BMP production in CL6 cells, expression levels of *Bmp2* and *Bmp4* were determined by quantitative real-time RT-PCR analysis (Fig. 4C). DMSO clearly induced the *Bmp2* and *Bmp4* genes, and DMSO-induction was inhibited by BMP2 protein. The expression level of *Bmp2* was highest during days 7–10 (Fig. 4C: *Bmp2*) in DMSO-induced CL6 cells, and that of *Bmp4* was highest during days 5–7 (Fig. 4C: *Bmp4*).

To investigate BMP signaling on cardiomyogenic differentiation, we used the *Id1* promoter-Lux plasmid that includes the luciferase gene driven by the *Id1* promoter, known as a BMP target promoter (Fig. 4D). DMSO increased BMP signaling activity that peaked at 5 days (Fig. 4D, open square). BMP2 protein increased BMP signaling activity at 3 days (Fig. 4D, closed square), but lost BMP signaling activity at 5 days and later, implying that this loss of BMP signaling leads to lack of cardiomyogenic induction.

Since Wnt/β-catenin signaling is involved in CL6 cardiomyogenesis [23,25], we hypothesized that the BMP effect on CL6 cardiomyogenesis is mediated through Wnt/β-catenin signaling. Expression of Wnt3a, an activator of canonical Wnt signaling, was indeed detected in CL6 cells exposed to DMSO, and BMP2 significantly down-regulated *Wnt3a* expression at day 3 (Fig. 4E). By using the TOPflash plasmid [23] which includes the luciferase gene driven by two sets of three copies of the TCF recognition site, Wnt/β-catenin signaling was assessed to investigate the effect of BMP2. Wnt/β-catenin signaling activity increased at 48 h after treatment with DMSO. Activity was increased by DMSO treatment but decreased by BMP2 (Fig. 4F). Time course analysis revealed that Wnt/β-catenin activity peaked at 5 days after DMSO treatment, and decreased thereafter (Fig. 4G). BMP2 inhibited DMSO-induced Wnt/β-catenin activity throughout the experimental period (up to 14 days). These results imply that BMP signaling inhibits CL6 cardiomyogenesis at the early stage through inhibition of Wnt/β-catenin signaling.

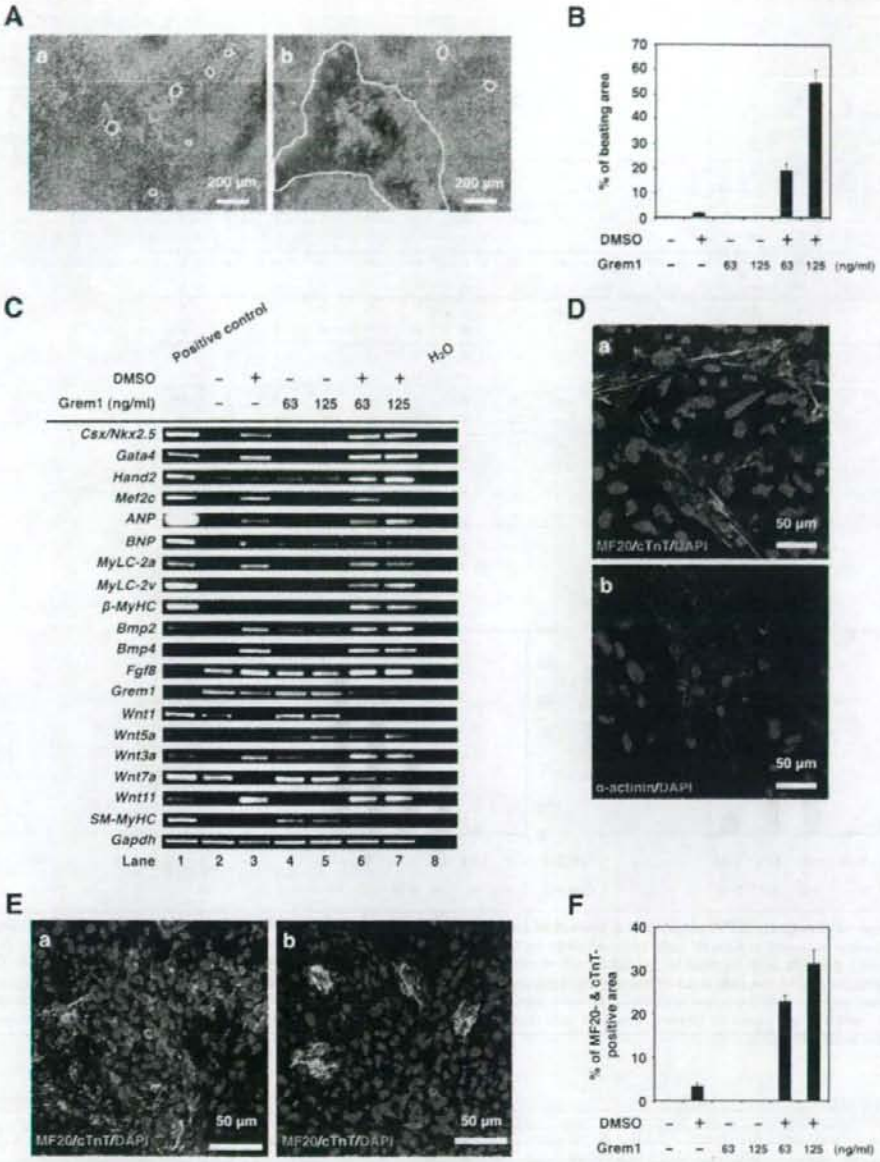

Figure 2. Grem1 enhanced cardiomyogenic differentiation in DMSO-induced CL6 cells. (A) Phase contrast micrograph of CL6 cells with exposure to DMSO alone (a), Grem1 (125 ng/ml) and DMSO (b) for 14 days. The medium, including Grem1 and DMSO, was changed every day. CL6 cells exhibited apparent spontaneous beating between days 9–11. Beating CL6 cell colonies are outlined by white lines. **(B)** Percentage of beating area in differentiated CL6 cells. CL6 cell treated with Grem1 (125 ng/ml) and DMSO exhibited the strongest contraction. **(C)** RT-PCR analysis of the genes encoding cardiac-specific transcriptional factors (*Csx/Nkx2.5*, *Gata4*, *Mef2c*, *Hand2*), circulating hormone (*ANP*, *BNP*), cardiac-specific proteins (*MyLC-2a*, *MyLC-2v*, *β-MyHC*), cytokines (*Bmp2*, *Bmp4*, *Fgf8*, *Grem1*, *Wnt1*, *Wnt3a*, *Wnt5a*, *Wnt7a*, *Wnt11*), *SM-MyHC*, and *Gapdh* (From top to bottom). Mouse total heart RNA for the *Csx/Nkx2.5*, *Gata4*, *Mef2c*, *Hand2*, *ANP*, *BNP*, *MyLC-2a*, *MyLC-2v*, *β-MyHC*, *Bmp2*, *Bmp4*, *Grem1*, *Wnt11*, *SM-MyHC*, and *Gapdh* genes, mouse embryonic stem cell RNA for the *Fgf8* gene, and mouse total skeletal muscle RNA for the *Wnt1*, *Wnt3a*, *Wnt5a*, and *Wnt7a* genes were used for positive controls. H_2O (without RNA) served as a negative control. **(D)** Immunocytochemistry of CL6 cells 14 days after exposure to Grem1 (125 ng/ml) and DMSO with MF20 and cTnT (a), and α-actinin (b). Cell nuclei are stained with DAPI. Clear striations are evident. **(E)** Immunocytochemistry of CL6 cells 14 days after exposure to Grem1 and DMSO with cardiac troponin T (cTnT) and sarcomeric myosin (MF20). CL6 cells treated with Grem1 (125 ng/ml) and DMSO (a), and DMSO alone (b) stained positive for cTnT and MF20. Untreated CL6 cells, i.e. not exposed to Grem1(125 ng/ml) or DMSO, stained negative for cTnT and MF20. Cell nuclei were stained with DAPI. **(F)** Percentage of MF20- and cTnT-double positive area.

doi:10.1371/journal.pone.0002407.g002

A

	Day	0	1	2	3	4	5	6	7	8	9	10	11	12	13	14
DMSO	–	–	–	–	–	–	–	–	–	–	–	–	–	–	–	–
Grem1	–	–	–	–	–	–	–	–	–	–	–	–	–	–	–	–
DMSO	1-14	–	+	+	+	+	+	+	+	+	+	+	+	+	+	+
Grem1	–	–	–	–	–	–	–	–	–	–	–	–	–	–	–	–
DMSO	1-14	–	+	+	+	+	+	+	+	+	+	+	+	+	+	+
Grem1	1-3	–	+	+	+	–	–	–	–	–	–	–	–	–	–	–
DMSO	1-14	–	+	+	+	+	+	+	+	+	+	+	+	+	+	+
Grem1	4-7	–	–	–	–	+	+	+	+	–	–	–	–	–	–	–
DMSO	1-14	–	+	+	+	+	+	+	+	+	+	+	+	+	+	+
Grem1	8-14	–	–	–	–	–	–	–	–	+	+	+	+	+	+	+
DMSO	1-3		+	+	+	–	–	–	–	–	–	–	–	–	–	–
Grem1	–	–	–	–	–	–	–	–	–	–	–	–	–	–	–	–
DMSO	1-14	–	+	+	+	+	+	+	+	+	+	+	+	+	+	+
Grem1	1-14	–	+	+	+	+	+	+	+	+	+	+	+	+	+	+
DMSO	1-14	–	+	+	+	+	+	+	+	+	+	+	+	+	+	+
Grem1	1-3	–	+	+	+	–	–	–	–	–	–	–	–	–	–	–
DMSO	1-3	–	+	+	+	–	–	–	–	–	–	–	–	–	–	–
Grem1	1-3	–	+	+	+	–	–	–	–	–	–	–	–	–	–	–

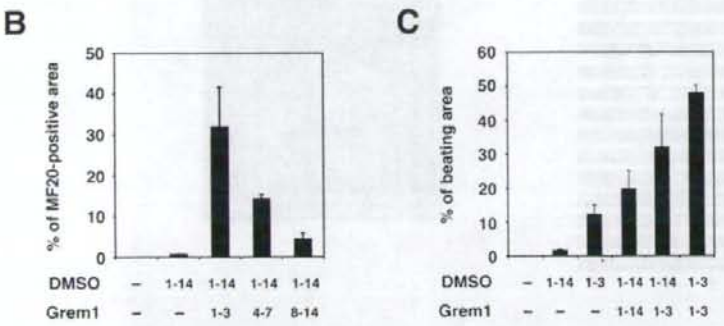

Figure 3. Percentage of myogenic differentiation by period of treatment with Grem1 in CL6 cells. (A) Protocol for treatment of Grem1 and DMSO. CL6 cells were passaged at 1.8×10^5 cells in 6-well plate on Day 0. CL6 cells were exposed to Grem1 (125 ng/ml) and/or DMSO on the indicated day. Day when the cells were exposed to the inducers is shown by "+" (in gray cells for clarity). The medium including Grem1 and DMSO was changed every day. On day 14, the cells were immunocytochemically stained with MF20 antibody. **(B)** Myogenic differentiation of CL6 cells was estimated by sarcomeric myosin (MF20)-positive area. CL6 cells were treated with Grem1 (125 ng/ml) and DMSO for the indicated days. **(C)** Myogenic differentiation of CL6 cells was estimated by beating area. CL6 cells treated with DMSO and Grem1 (125 ng/ml) were incubated at indicated days.
doi:10.1371/journal.pone.0002407.g003

Discussion

Our bioinformatics study using the results from the global gene expression analysis of human cells (GSM412342-41344 and GSM201137-201145 at http://www.ncbi.nlm.nih.gov/geo) nominated Grem1 as a candidate gene that may participate in cardiomyogenesis. By using CL6 embryonic cells as a model of cardiomyogenesis, we obtained two major findings: the first is that Grem1 enhanced cardiomyogenic differentiation of DMSO-induced CL6 cells at the early stage; the second is that Wnt/β-catenin and BMP signaling activity had developmental stage-specific effects on cardiomyogenesis (Fig. 5). Wnt/β-catenin activity at the early stage enhanced embryonic cell differentiation into cardiomyocytes, while suppressing this activity by BMP2 or BMP4 proteins as reported in the avian embryo [26]. In contrast, BMP signaling activity in the late stage enhanced cardiomyocytic differentiation. Grem1 regulated the stage-specific Wnt/β-catenin and BMP signaling activity on cardiomyogenesis.

Many studies have indicated that Grem1 is involved in cell differentiation and development, such as osteogenesis [27], lung morphogenesis [28], myogenesis [29], and limb formation [30], through inhibition of BMP2 and BMP4. Grem1-null mice show intact heart development, despite impairment of lung and kidney [31], and therefore Grem1 is considered not to be involved in cardiogenesis, or supplementary factors such as Noggin [32], with a similar function, may compensate Grem1 during development. Grem1 had an enhancing or promoting activity in *in vitro* cardiomyogenesis, as is the case with platelet-derived growth factor as a promoter of cell growth [33]. In this study, Grem1 was involved in cardiomyocyte differentiation. However Grem1 alone could not induce cardiomyocytic differentiation of CL6 cells in the absence of DMSO (Fig. 2C and F), suggesting that Grem1 is solely

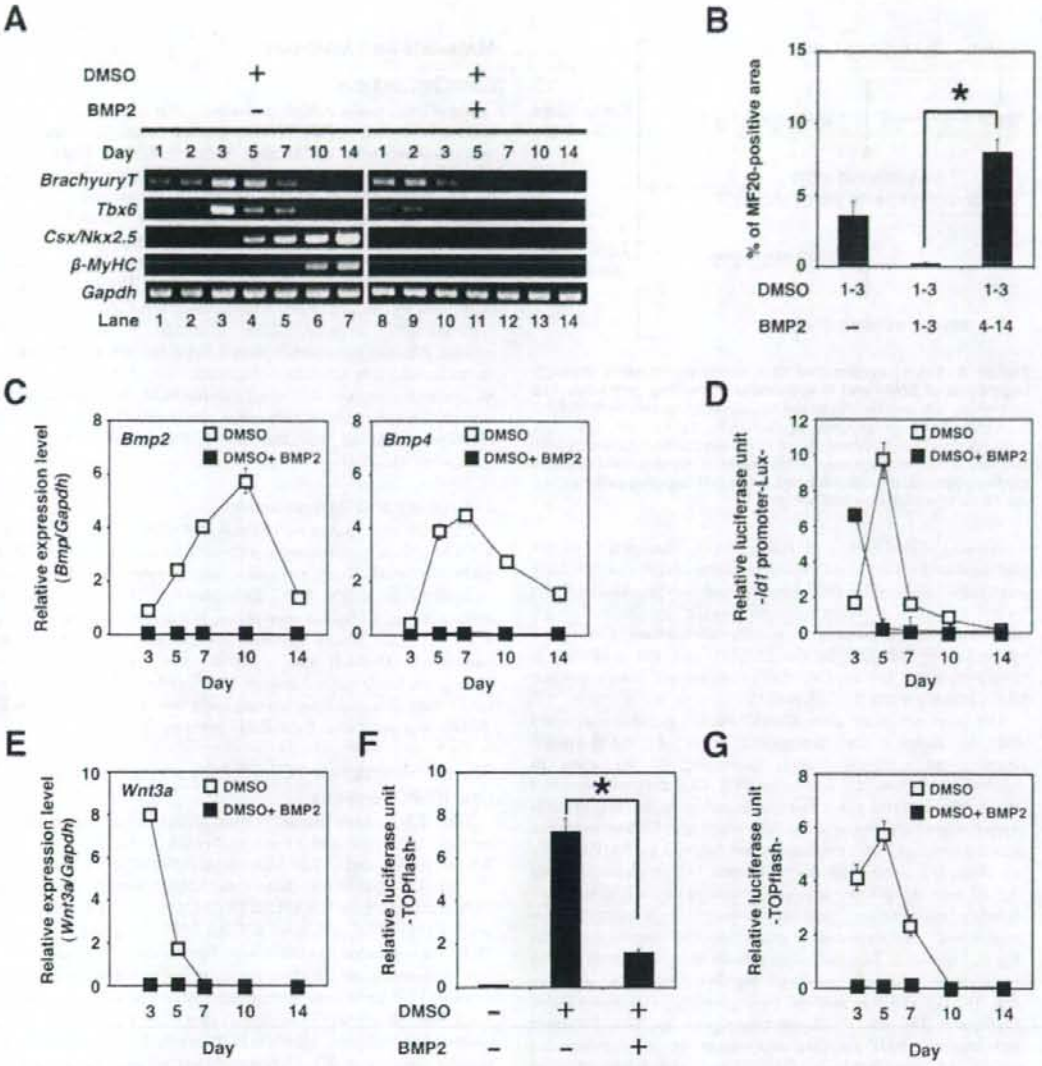

Figure 4. Cardiomyogenic differentiation in CL6 cells (days 1–3) is inhibited by BMP2. (A) RT-PCR analysis of the gene encoding *BrachyuryT*, *Tbx6*, cardiac-specific transcriptional factor (*Csx/Nkx2.5*), cardiac-specific protein (*β-MyHC*), and *Gapdh* (From top to bottom) of CL6 cells treated with DMSO alone, or DMSO and BMP2 (100 ng/ml) for the first 3 days (days 1–3). The medium, including BMP2 and DMSO, was changed every day. **(B)** Percentage of MF20-positive area. Immunocytochemistry was carried out on CL6 cells 14 days after cells had been exposed to DMSO and BMP2 (100 ng/ml) for the first 3 days (days 1–3). The asterisk indicates a significant statistical difference ($P<0.05$). **(C)** Quantitative real-time RT-PCR analysis of the gene encoding *Bmp2* (left), and *Bmp4* (right) in CL6 cells treated with DMSO alone (open square), or DMSO and BMP2 (100 ng/ml) (closed square) for the first 3 days (days 1–3). **(D)** BMP signaling activity of CL6 cells treated with DMSO alone (open square), or DMSO and BMP2 (100 ng/ml) (closed square) for the first 3 days (days 1–3) were determined by luciferase activity analysis using *Id1* promoter-Lux (a firefly luciferase reporter plasmid driven by the Id1 binding sites), pRL-CMV as co-transfected control, and Dual luciferase reporter assay system. Relative luciferase unit of the CL6 cells untreated with inducers at day 3 is regarded as 0.1 (data not shown). **(E)** Quantitative real-time RT-PCR analysis of the gene encoding *Wnt3a* in CL6 cells treated with DMSO alone (open square), or DMSO and BMP2 (100 ng/ml) (closed square) for the first 3 days (days 1–3). **(F)** Wnt/β-catenin signaling activity of CL6 cells 48 h after exposure to DMSO, or DMSO and BMP2 (100 ng/ml) was determined by luciferase activity analysis using TOPflash (a firefly luciferase reporter plasmid driven by two sets of three copies of the TCF binding site and herpes simple virus thymidine kinase minimal promoter), pRL-CMV as co-transfected control, and Dual luciferase reporter assay system. Relative luciferase unit of the CL6 cells untreated with inducers is regarded as 0.1. The asterisk indicates a significant statistical difference ($P<0.05$). **(G)** Timeframe of Wnt/β-catenin signaling activity in CL6 cells treated with DMSO alone (open square), or DMSO and BMP2 (100 ng/ml) (closed square) for the first 3 days (days 1–3). Relative luciferase unit of the CL6 cells untreated with inducers at day 3 is regarded as 0.1 (data not shown).
doi:10.1371/journal.pone.0002407.g004

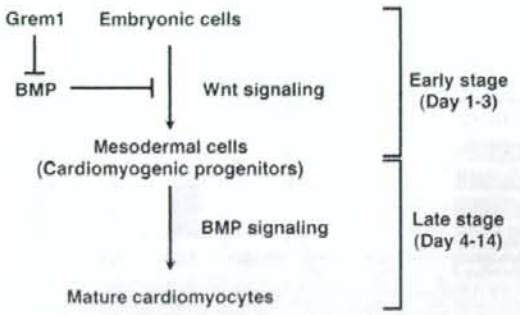

Figure 5. Grem1-accelerated CL6 cardiomyogenesis through regulation of BMP- and Wnt/β-catenin-signaling pathways. CL6 embryonic cells start to differentiate into mesodermal cells through Wnt/β-catenin signaling pathway at the early stage (days 1–3), and mesodermal CL6 cells differentiate into mature cardiomyocytes by BMP pathway at the late stage (days 4–14). Grem1 accelerates DMSO-induced cardiomyogenesis through inhibition of the BMP-signaling pathway.
doi:10.1371/journal.pone.0002407.g005

a promoter of cardiomyogenic differentiation. One of the possible mechanisms for Grem1-enhanced cardiomyogenesis at the early stage is inhibition of the BMP signaling pathway [3]. Alternatively, Grem1-enhanced cardiomyogenesis may be mediated through proliferation of cardiac progenitor cells, as is the case of myogenic progenitor proliferation by Grem1 [34], and this possibility is supported by an increased number of sarcomeric myosin-positive CL6 cardiomyocytes (Fig. 2E and F).

The stage specificity of the Grem1 effect is possibly correlated with the biphasic and antagonistic effect of Wnt/β-catenin signaling on cardiomyogenesis, depending on the stage of development *in vitro* [25] and *in vivo* [35]. CL6 cells differentiated into cardiomyocytes via mesodermal induction by the Wnt/β-catenin signaling pathway at the early stage, and CL6 mesodermal cells differentiated into cardiomyocytes induced by BMP2 at the late stage. It is conceivable that embryonic cells, such as CL6 cells and ES cells, differentiate into cardiomyocytes by inhibiting BMP signaling via putative "mesodermal cells" or "cardiomyogenic progenitors", or differentiation stages corresponding to these cells (Fig. 5, Figure S2). The early stage process from embryonic cells to mesodermal cells was mediated via Wnt/β-catenin signaling (Fig. 4F, G), and was assessed by expression of *BrachyuryT* and *Tbx6* genes (Fig. 4A), which are target genes for Wnt/β-catenin signaling [36]. BMP signaling antagonizes the cell fate-inducing activity of Wnt/β-catenin [37]. When embryonic cells or cardiomyogenic progenitors are induced to become mature cardiomyocytes by cytokines and growth factors, we must be careful with respect to the stage of cell differentiation because of the biphasic differential action of the factors which are dependent upon the differentiation stage.

In conclusion, we have demonstrated that Grem1 enhances the commitment or determined path to cardiogenic differentiation of CL6 teratocarcinoma cells. Apart from a role in development, Grem1 may serve a clinical use in cardiology, like granulocyte colony-stimulating factor that accelerates production of granulocytes in both peripheral blood and bone marrow. Nomination of *Grem1* as a cardiomyogenic factor is based on hierarchical clustering analysis using global gene expression data of human cells. This bioinformatics approach may be useful for identifying morphogens/factors that can induce differentiation of other cell types/tissues/organs.

Materials and Methods

GeneChip analysis

GeneChip analysis was performed (Fig. 1A, Table 1) as previously described [38]. Human genome-wide gene expression was examined with the Human Genome U133A Probe array (GeneChip; Affymetrix), which contains the oligonucleotide probe set for approximately 23,000 full-length genes and expressed sequence tags, according to the manufacturer's protocol (Expression Analysis technical manual and GeneChip Small Sample Target Labeling Assay version 2 technical note [http://www.affymetrix.com/support/technical/index.affx]). Data analysis was performed by the GeneChip Operation System (Affymetrix) and GeneSpringGX software (Silicon Genetics). To normalize the staining intensity variations between chips, the average difference values for all genes on a given chip were divided by the median of all measurements on that chip. Hierarchical-clustering analysis was performed using a minimum distance value of 0.001, a separation ratio of 0.5, and the standard definition of the correlation distance.

Cell culture and differentiation

CL6 cells were grown on 100 mm dishes (Becton Dickinson) in α-MEM (Gibco) supplemented with 10% fetal bovine serum (FBS) (JRH Bioscience, Inc.), penicillin, and streptomycin, and were maintained in a 5% CO_2 atmosphere at 37°C. To induce differentiation, CL6 cells were plated at a density of 1.8×10^5 cells in a 6-well plate (Becton Dickinson) or gelatin-coated 35 mm glass base dishes (IWAKI) with α-MEM containing Grem1 (63 or 125 ng/ml: R&D system) and/or 1% dimethyl sulfoxide (DMSO) for 14 days. Recombinant human bone morphogenetic protein-2 (BMP2) was purchased from R&D systems.

Reverse transcriptase-PCR (RT-PCR) and quantitative real-time RT-PCR analysis

Total RNAs were extracted from differentiated and undifferentiated CL6 cells and mouse embryonic stem (ES) cells with RNeasy minikit and DNase I treatment (QIAGEN). Mouse ES cell (129 strains) RNA, mouse heart total RNA (Clontech) and mouse skeletal muscle/total RNA (UNITECH. Co., Ltd.) were used as a positive control for each primer. Total RNA (2.0 μg each) for RT-PCR was converted to cDNA with Superscript™ III RNase H– reverse transcriptase (Invitrogen), according to the manufacturer's manual. PCR conditions were optimized and linear amplification range was determined for each primer by varying annealing temperature and cycle number. PCR products were identified by positive control size. RT-PCR was performed using the primers of the genes of cardiac specific transcription factors: *Csx/Nkx2.5*, *Gata4*, *Mef2c*, *Hand2*; circulating hormone: *ANP*, *BNP*; cardiac structural proteins: *β-MyHC*, *MyLC-2a*, *MyLC-2v*; cytokines: *Bmp2*, *Bmp4*, *Fgf8*, *Grem1*, *Wnt1*, *Wnt5a*, *Wnt5a*, *Wnt7a*, *Wnt11*; smooth muscle structural protein: smooth muscle-myosin heavy chain (*SM-MyHC*); the early mesodermal marker: *BrachyuryT*, *T-box6* (*Tbx6*); and *Gapdh* as control. PCR was performed with exTaq DNA polymerase and exTaq PCR buffer (TaKaRa) or LATaq DNA polymerase and GC buffer I (TaKaRa) for 25 or 30 cycles, with each cycle consisting of 95°C for 30 s, 50°C, 55°C, 60°C or 65°C for 45 s, and 72°C for 45 s, with an additional 5 min incubation at 72°C after completion of the final cycle. PCR primers for the genes of *Csx/Nkx2.5*, *Gata4*, *Mef2c*, *Hand2*, *ANP*, *BNP*, *β-MyHC*, *MyLC-2a*, *MyLC-2v*, *Bmp2*, *Bmp4*, *Fgf8*, *Grem1*, *Wnt1*, *Wnt3a*, *Wnt5a*, *Wnt7a*, *Wnt11*, *SM-MyHC*, *BrachyuryT*, *Tbx6*, and *Gapdh* (Table S1a) were obtained from Mouse Genome

Informatics (http://www.informatics.jax.org/). The PCR products were size-fractionated by 2% agarose gel electrophoresis.

Quantitative real-time RT-PCR was performed on an ABI Prism 7700 Sequence Detection System (Applied Biosystems), using 100 ng of cDNA in 25 μl reaction volume with 10 nmol/l of each primer, and 12.5 μl SYBR Green Realtime PCR Master Mix (TOYOBO). PCR primers for the genes of *Bmp2*, *Bmp4*, *Wnt3a*, and *Gapdh* (Table S1b) were obtained from PrimerBank (http://pga.mgh.harvard.edu/primerbank/index.html). Calculations were automatically performed by ABI software (Applied BioSystems).

Immunocytochemistry

A laser confocal microscope (LSM510, Zeiss) was used for immunocytochemical analysis. Differentiated and undifferentiated CL6 cells were fixed with 4% paraformaldehyde (Wako) for 5 min at 4°C and treated with 0.1% triton X-100 (Sigma) in PBS for 20 min at room temperature, then incubated for 20 min at room temperature in a protein-blocking solution consisting of PBS supplemented with 5% normal goat serum (DakoCytomation). These CL6 cells were then incubated overnight with primary antibody monoclonal anti-sarcomeric myosin antibody (MF20, mouse IgG_{2b} isotype, 1 mg/ml, University of Iowa Hybridoma Bank) and Troponin T, and Cardiac Isoform Ab-1 clone 13-11 (cTnT, mouse IgG_1 isotype, 1:300, Lab Vision Corp), or the monoclonal anti-α-actinin (SARCOMERIC) CLONE EA-53 (α-actinin, mouse IgG_1 isotype, 1:300, Sigma) in PBS at 4°C. The cells were extensively washed in PBS and incubated at room temperature with Alexa Fluor 568-conjugated goat anti-Mouse IgG_{2b} (anti-MF20) (Molecular Probe; diluted 1:300), Alexa Fluor 488-conjugated goat anti-mouse IgG_1 (anti-cTnT) (Molecular Probe; diluted 1:300), Alexa Fluor 546-conjugated goat anti-mouse IgG(H+L) (anti-α-actinin) (Molecular Probe; diluted 1:300), and nuclei were counterstained with 4′, 6-diamidino-2-phenylindole (DAPI) (Wako; diluted 1:300) for 45 min. To prevent fading, cells were then mounted in DakoCytomation Fluorescent Mounting Medium (DakoCytomation).

Transfection and luciferase assays

Cells (8.0×10^5) seeded and cultured in 60 mm dishes (Becton Dickinson) were transfected 18 h after plating using Lipofectamine 2000 (Invitrogen) and PLUS reagent (Invitrogen) in Opti-MEM (Gibco). Transfection contained 1.0 μg of TOPflash plasmid (Upstate Biotechnology) for measurement of Wnt/β-catenin activity, or 5.0 μg of the *Id1* promoter-Lux plasmid (provided by Dr Imamura and Dr Miyazono) for measurement of BMP-induced *Id1* gene transcription, and 0.5 μg of pRL-CMV (Promega) as co-transfected control. Medium containing 10% FBS was changed 3 h after transfection and transfected cells (1.8×10^5) were re-seeded in 6-well plates 24 h after transfection. After 18 h, CL6 cells were induced with BMP2 (100 ng/ml) and DMSO. CL6 cells were prepared for luciferase activity analysis using Dual luciferase reporter assay system (Promega).

Area calculation

The regions of interest (beating area, immunostaining area) were defined in Photoshop (Adobe systems) using the 'magic wand' tool. The total numbers of pixels identified were then counted using the histogram function. At least five different fields were measured for each dish.

Statistical analysis

Results, shown as the mean±SE, were compared by ANOVA followed by Scheffé's test, with $P<0.05$ considered significant.

Supporting Information

Figure S1 A semi-quantitative RT-PCR of cardiomyocyte-specific genes. To investigate expression level of cardiomyocyte-specific genes (Csx/Nkx2.5, Gata4, MyLC-2a, and MyLC-2v), a semi-quantitative RT-PCR was performed from CL6 cells treated with 1% DMSO and the indicated concentration of Grem1 for 14 days. Each RT-PCR product was electrophoresed in 2% agarose gel, and was measured using ImageJ software (http://rsb.info.nih.gov/ij/) to calculate the ratio of each gene to Gapdh. The expression level for each gene is determined relative to that of Gapdh, and expression level in CL6 cells treated with DMSO alone was regarded as 1.0. The relative expression levels were averaged from at least three independent experiments.
Found at: doi:10.1371/journal.pone.0002407.s001 (1.04 MB DOC)

Figure S2 Grem1 enhanced cardiomyogenic differentiation of mouse ES cells. Mouse ES cells (NCH1.5, C57BL/6J×129ter/Sv) were cultured on a mouse embryonic fibroblast feeder layer inactivated with 30 Gy γ-irradiation in gelatin-coated 60 mm dishes (Becton, Dickinson). Cells were grown in KnockOut DMEM (Gibco) supplemented with 15% fetal bovine serum (Cell Culture Technologies), 2 mM GlutaMAX (Gibco), 0.1 mM non-essential amino acid (Gibco), 0.1 mM 2-mercaptoethanol (Gibco), penicillin, streptomycin, and 2,000 U/ml mouse leukemia inhibitory factor (LIF) (Chemicon). For cardiomyogenic differentiation, ES cells were exposed to 125 ng/ml Grem1 (R&D systems) for the three days. The cells were then trypsinized and cultured to form embryonic bodies (EBs) from a single cell using a three-dimensional culture system (without LIF) on low cell binding dishes (96-well plate round bottom). This represented day 0 of EB formation. On the next day, the medium was replaced with the same medium without LIF. EBs were re-seeded on gelatin-coated 48-well plates with one EB per well, on day 8 after the start of EB formation. The cardiomyogenic induction was estimated by the beating EB number per total EB number, measured on day 12 under a phase-contrast microscope. Grem1 increased the percentage of beating EBs to 69.2%, as compared with 26.7% in EBs without Grem1 treatment. The numbers in parentheses indicate the EB numbers counted.
Found at: doi:10.1371/journal.pone.0002407.s002 (1.27 MB DOC)

Table S1 Primer sequences.
Found at: doi:10.1371/journal.pone.0002407.s003 (0.06 MB DOC)

Movie S1 CL6 cells treated with DMSO alone. P19CL6 cells are reproducibly and stably induced into beating cardiomyocytes with DMSO.
Found at: doi:10.1371/journal.pone.0002407.s004 (1.66 MB MOV)

Movie S2 CL6 cells treated with Grem1 (125 ng/ml) and DMSO. Grem1 dramatically promotes DMSO-induced cardiomyogenic differentiation of P19CL6 cells at a concentration of 125 ng/ml.
Found at: doi:10.1371/journal.pone.0002407.s005 (2.40 MB MOV)

Acknowledgments

We would like to express our sincere thanks to T. Imamura and K. Miyazono for the *Id1* promoter-Lux plasmid, and J. Fujimoto for their discussion of this work.

Author Contributions

Conceived and designed the experiments: AU DK. Performed the experiments: DK HM RI KM. Analyzed the data: AU AN DK YT RI MT MW. Contributed reagents/materials/analysis tools: IK AN IS HS. Wrote the paper: AU DK.

References

1. Andree B, Duprez D, Vorbusch B, Arnold HH, Brand T (1998) BMP-2 induces ectopic expression of cardiac lineage markers and interferes with somite formation in chicken embryos. Mech Dev 70: 119–131.
2. Schultheiss TM, Burch JB, Lassar AB (1997) A role for bone morphogenetic proteins in the induction of cardiac myogenesis. Genes Dev 11: 451–462.
3. Angello JC, Kaestner S, Welikson RE, Buskin JN, Hauschka SD (2006) BMP induction of cardiogenesis in P19 cells requires prior cell-cell interaction(s). Dev Dyn 235: 2122–2133.
4. Alsan BH, Schultheiss TM (2002) Regulation of avian cardiogenesis by Fgf8 signaling. Development 129: 1935–1943.
5. Crossley PH, Martin GR (1995) The mouse Fgf8 gene encodes a family of polypeptides and is expressed in regions that direct outgrowth and patterning in the developing embryo. Development 121: 439–451.
6. Reifers F, Walsh EC, Leger S, Stainier DY, Brand M (2000) Induction and differentiation of the zebrafish heart requires fibroblast growth factor 8 (fgf8/acerebellar). Development 127: 225–235.
7. Whitehead GG, Makino S, Lien CL, Keating MT (2005) fgf20 is essential for initiating zebrafish fin regeneration. Science 310: 1957–1960.
8. Yamagishi H, Olson EN, Srivastava D (2000) The basic helix-loop-helix transcription factor, dHAND, is required for vascular development. J Clin Invest 105: 261–270.
9. Ariizumi T, Kinoshita M, Yokota C, Takano K, Fukuda K, et al. (2003) Amphibian in vitro heart induction: a simple and reliable model for the study of vertebrate cardiac development. Int J Dev Biol 47: 405–410.
10. Gavert N, Ben-Ze'ev A (2007) beta-Catenin signaling in biological control and cancer. J Cell Biochem 102: 820–828.
11. Chien KR, Moretti A, Laugwitz KL (2004) Development. ES cells to the rescue. Science 306: 239–240.
12. Pandur P, Lasche M, Eisenberg LM, Kuhl M (2002) Wnt-11 activation of a non-canonical Wnt signalling pathway is required for cardiogenesis. Nature 418: 636–641.
13. Yamagishi H, Yamagishi C, Nakagawa O, Harvey RP, Olson EN, et al. (2001) The combinatorial activities of Nkx2.5 and dHAND are essential for cardiac ventricle formation. Dev Biol 239: 190–203.
14. Park M, Wu X, Golden K, Axelrod JD, Bodmer R (1996) The wingless signaling pathway is directly involved in Drosophila heart development. Dev Biol 177: 104–116.
15. Marvin MJ, Di Rocco G, Gardiner A, Bush SM, Lassar AB (2001) Inhibition of Wnt activity induces heart formation from posterior mesoderm. Genes Dev 15: 316–327.
16. Schneider VA, Mercola M (2001) Wnt antagonism initiates cardiogenesis in Xenopus laevis. Genes Dev 15: 304–315.
17. Tzahor E, Lassar AB (2001) Wnt signals from the neural tube block ectopic cardiogenesis. Genes Dev 15: 255–260.
18. Olson EN (2001) Development. The path to the heart and the road not taken. Science 291: 2327–2328.
19. Terami H, Hidaka K, Katsumata T, Iio A, Morisaki T (2004) Wnt11 facilitates embryonic stem cell differentiation to Nkx2.5-positive cardiomyocytes. Biochem Biophys Res Commun 325: 968–975.
20. Sharov AA, Dudekula DB, Ko MS (2005) A web-based tool for principal component and significance analysis of microarray data. Bioinformatics 21: 2548–2549.
21. Hamatani T, Carter MG, Sharov AA, Ko MS (2004) Dynamics of global gene expression changes during mouse preimplantation development. Dev Cell 6: 117–131.
22. Sharov AA, Dudekula DB, Ko MSH (2005) http://lgsun.grc.nia.nih.gov/ANOVA/help.html#hierarchical Accessed 2007 April 20. Bioinformatics Advance Access.
23. Naito AT, Akazawa H, Takano H, Minamino T, Nagai T, et al. (2005) Phosphatidylinositol 3-kinase-Akt pathway plays a critical role in early cardiomyogenesis by regulating canonical Wnt signaling. Circ Res 97: 144–151.
24. Hsu DR, Economides AN, Wang X, Eimon PM, Harland RM (1998) The Xenopus dorsalizing factor Gremlin identifies a novel family of secreted proteins that antagonize BMP activities. Mol Cell 1: 673–683.
25. Naito AT, Shiojima I, Akazawa H, Hidaka K, Morisaki T, et al. (2006) Developmental stage-specific biphasic roles of Wnt/beta-catenin signaling in cardiomyogenesis and hematopoiesis. Proc Natl Acad Sci U S A 103: 19812–19817.
26. Jin EJ, Erickson CA, Takada S, Burrus LW (2001) Wnt and BMP signaling govern lineage segregation of melanocytes in the avian embryo. Dev Biol 233: 22–37.
27. Sutherland MK, Geoghegan JC, Yu C, Turcott E, Skonier JE, et al. (2004) Sclerostin promotes the apoptosis of human osteoblastic cells: a novel regulation of bone formation. Bone 35: 828–835.
28. Shi W, Zhao J, Anderson KD, Warburton D (2001) Gremlin negatively modulates BMP-4 induction of embryonic mouse lung branching morphogenesis. Am J Physiol Lung Cell Mol Physiol 280: L1030–1039.
29. Tzahor E, Kempf H, Mootoosamy RC, Poon AC, Abzhanov A, et al. (2003) Antagonists of Wnt and BMP signaling promote the formation of vertebrate head muscle. Genes Dev 17: 3087–3099.
30. Zuniga A, Michos O, Spitz F, Haramis AP, Panman L, et al. (2004) Mouse limb deformity mutations disrupt a global control region within the large regulatory landscape required for Gremlin expression. Genes Dev 18: 1553–1564.
31. Michos O, Panman L, Vintersten K, Beier K, Zeller R, et al. (2004) Gremlin-mediated BMP antagonism induces the epithelial-mesenchymal feedback signaling controlling metanephric kidney and limb organogenesis. Development 131: 3401–3410.
32. Yuasa S, Itabashi Y, Koshimizu U, Tanaka T, Sugimura K, et al. (2005) Transient inhibition of BMP signaling by Noggin induces cardiomyocyte differentiation of mouse embryonic stem cells. Nat Biotechnol 23: 607–611.
33. Singh JP, Chalkin MA, Pledger WJ, Scher CD, Stiles CD (1983) Persistence of the mitogenic response to platelet-derived growth factor (competence) does not reflect a long-term interaction between the growth factor and the target cell. J Cell Biol 96: 1497–1502.
34. Frank NY, Kho AT, Schatton T, Murphy GF, Molloy MJ, et al. (2006) Regulation of myogenic progenitor proliferation in human fetal skeletal muscle by BMP4 and its antagonist Gremlin. J Cell Biol 175: 99–110.
35. Klaus A, Saga Y, Taketo MM, Tzahor E, Birchmeier W (2007) Distinct roles of Wnt/beta-catenin and Bmp signaling during early cardiogenesis. Proc Natl Acad Sci U S A 104: 18531–18536.
36. Yamaguchi TP, Takada S, Yoshikawa Y, Wu N, McMahon AP (1999) T (Brachyury) is a direct target of Wnt3a during paraxial mesoderm specification. Genes Dev 13: 3185–3190.
37. Kleber M, Lee HY, Wurdak H, Buchstaller J, Riccomagno MM, et al. (2005) Neural crest stem cell maintenance by combinatorial Wnt and BMP signaling. J Cell Biol 169: 309–320.
38. Sugiki T, Uyama T, Toyoda M, Morioka H, Kume S, et al. (2007) Hyaline cartilage formation and enchondral ossification modeled with KUM5 and OP9 chondroblasts. J Cell Biochem 100: 1240–1254.

Nicotine Acts on Growth Plate Chondrocytes to Delay Skeletal Growth through the α7 Neuronal Nicotinic Acetylcholine Receptor

Atsuo Kawakita[1,2], Kazuki Sato[2], Hatsune Makino[1], Hiroyasu Ikegami[2], Shinichiro Takayama[3], Yoshiaki Toyama[2], Akihiro Umezawa[1]*

1 Department of Reproductive Biology, National Institute for Child Health and Development, Tokyo, Japan, 2 Department of Orthopaedic Surgery, Keio University School of Medicine, Tokyo, Japan, 3 Department of Orthopaedic Surgery, National Center for Child Health and Development, Tokyo, Japan

Abstract

Background: Cigarette smoking adversely affects endochondral ossification during the course of skeletal growth. Among a plethora of cigarette chemicals, nicotine is one of the primary candidate compounds responsible for the cause of smoking-induced delayed skeletal growth. However, the possible mechanism of delayed skeletal growth caused by nicotine remains unclarified. In the last decade, localization of neuronal nicotinic acetylcholine receptor (nAChR), a specific receptor of nicotine, has been widely detected in non-excitable cells. Therefore, we hypothesized that nicotine affect growth plate chondrocytes directly and specifically through nAChR to delay skeletal growth.

Methodology/Principal Findings: We investigated the effect of nicotine on human growth plate chondrocytes, a major component of endochondral ossification. The chondrocytes were derived from extra human fingers. Nicotine inhibited matrix synthesis and hypertrophic differentiation in human growth plate chondrocytes in suspension culture in a concentration-dependent manner. Both human and murine growth plate chondrocytes expressed alpha7 nAChR, which constitutes functional homopentameric receptors. Methyllycaconitine (MLA), a specific antagonist of alpha7 nAChR, reversed the inhibition of matrix synthesis and functional calcium signal by nicotine in human growth plate chondrocytes in vitro. To study the effect of nicotine on growth plate in vivo, ovulation-controlled pregnant alpha7 nAChR +/− mice were given drinking water with or without nicotine during pregnancy, and skeletal growth of their fetuses was observed. Maternal nicotine exposure resulted in delayed skeletal growth of alpha7 nAChR +/+ fetuses but not in alpha7 nAChR −/− fetuses, implying that skeletal growth retardation by nicotine is specifically mediated via fetal alpha7 nAChR.

Conclusions/Significance: These results suggest that nicotine, from cigarette smoking, acts directly on growth plate chondrocytes to decrease matrix synthesis, suppress hypertrophic differentiation via alpha7 nAChR, leading to delayed skeletal growth.

Citation: Kawakita A, Sato K, Makino H, Ikegami H, Takayama S, et al. (2008) Nicotine Acts on Growth Plate Chondrocytes to Delay Skeletal Growth through the α7 Neuronal Nicotinic Acetylcholine Receptor. PLoS ONE 3(12): e3945. doi:10.1371/journal.pone.0003945

Editor: Rory Edward Morty, University of Giessen Lung Center, Germany

Received August 6, 2008; **Accepted** November 8, 2008; **Published** December 16, 2008

Copyright: © 2008 Kawakita et al. This is an open-access article distributed under the terms of the Creative Commons Attribution License, which permits unrestricted use, distribution, and reproduction in any medium, provided the original author and source are credited.

Funding: This study was supported by a grant from the Smoking Research Foundation; by grants from the Ministry of Education, Culture, Sports, Science, and Technology (MEXT) of Japan; by the Ministry of Health, Labour and Welfare (MHLW) Sciences Research Grants; by a Research Grant on Health Science focusing on Drug Innovation from the Japan Health Science Foundation; by the program for promotion of Fundamental Studies in Health Science of the Pharmaceuticals and Medical Devices Agency; by a Research Grant for Cardiovascular Disease from the MHLW; and by a Grant for Child Health and Development from the MHLW. The funders had no role in study design, data collection and analysis, decision to publish, or preparation of the manuscript.

Competing Interests: The authors have declared that no competing interests exist.

* E-mail: umezawa@1985.jukuin.keio.ac.jp

Introduction

Though detrimental effects of cigarette smoking to the human body have been widely demonstrated, the effects on endochondral ossification are not well understood. Epidemiologically, maternal smoking reduces the height of newborns [1–5]. However, there are controversial views regarding the mechanisms behind delayed skeletal growth caused by cigarette smoking. The socioeconomic status of smoking mothers [6,7], deficient maternal diet [8], chronic hypoxia caused by carbon monoxide [9], impaired placental size and function, and decreased blood flow of placenta caused by nicotine [10] have all been reported as a possible causal factors responsible for reduction in height of newborns. Conversely, it has also been reported that socioeconomic status [11], maternal diet [12], and hypoxia are not responsible for the cause of delayed skeletal growth. Research suggests that smoking not only reduces body length but also brings ossification retardation in the rat smoking model [13]. Moreover, smoking delays chondrogenesis in a mouse model of fracture healing [14]. Cigarette smoking, thus, adversely affects endochondral ossification somehow during the course of skeletal growth and repair in animal models.

Among a multitude of chemicals and physiological functions arising from cigarette smoking, nicotine is one of the leading candidates for causing small newborns. Epidemiologically, nicotine content in cigarette is related to reduced birth length in humans [15]. However, the possible mechanism of delayed skeletal growth caused by nicotine remains unclarified. In this study, we investigated the effect of nicotine on growth plate chondrocytes, the principle

component of endochondral ossification. In the last decade, localization of neuronal nicotinic acetylcholine receptor (nAChR), a specific receptor of nicotine, has been widely detected in non-excitable cells [16]. Therefore, we hypothesized that nicotine affect growth plate chondrocytes directly and specifically through nAChR to delay skeletal growth. We here demonstrate that nicotine affected growth plate chondrocytes through alpha7 nAChR to decrease matrix synthesis and to suppress hypertrophic differentiation, thereby delaying skeletal growth.

Results

Detection and localization of nAChR in growth plate chondrocytes

To date, many epidemiological [1–5] and experimental [13] studies suggested that endochondral ossification is affected by cigarette smoking, especially by its major component, nicotine [15]. We thus assumed that nicotine may directly affect chondrocytes, a key player in endochondral ossification. To investigate whether the impact of nicotine on chondrocytes is specific, we studied the expression pattern of the specific receptor, nAChR. For screening of the existing subunits of nAChR, RT-PCR was performed with primers for each subunit of nAChR. Human growth plate chondrocytes expressed alpha5, alpha7, beta1 and epsilon subunits of nAChR (Figure 1A).

Among the detected subunits, only the alpha7 subunit can form a functional nAChR by forming a homopentameric receptor [17]. We thus tried to detect alpha7 subunit at a protein level. Western blot analysis revealed that chondrocytes produced alpha7 nAChR (Figure 1B). Immunocytochemical analysis also revealed that chondrocytes stained positive for alpha7 nAChR (Figure 1C). Moreover, the alpha7 subunit was detected at resting, proliferating and pre-hypertrophic chondrocytes of murine growth plate but not hypertrophic chondrocytes (Figure 1D). These results suggest that the growth plate chondrocytes in their non-hypertrophic stage express alpha7 homopentameric nAChR.

Effect of nicotine on chondrocytes cultured in agarose gel

To study the effect of nicotine on growth plate chondrocytes in vitro, two methods of suspension cultures, i.e., agarose gel culture and alginate bead culture, were employed. In agarose gel, the chondrocytes are initially embedded in the suspension layer solitarily. The chondrocytes then proliferate, differentiate, and aggregate to form a colony in the presence of ascorbic acid, and start to produce a matrix around themselves [18]. We applied the agarose gel culture to study the effect of nicotine on the proliferation and differentiation of growth plate chondrocytes in vitro. Nicotine was added to culture media for three weeks culture period. Nicotine decreased the percentage of colonies which produce matrix, as revealed by alcian blue (ALB) stains in a concentration-dependent manner (Figure 2A, upper panels). Similarly, nicotine suppressed Col X expression and enzyme activity of alkaline phosphatase (ALP) in a concentration-dependent manner (Figure 2A, middle and lower row panels). In contrast, nicotine did not affect colony density (Figure 2B, left panel) or the number of cells per colony (Figure 2B, right panel) which are indicators for cell proliferation. No nicotinic effect on cell proliferation was detected as assessed by immunohistochemistry using antibody to proliferating cell nuclear antigen (PCNA) (Figure S1). These results suggest that nicotine decreases the matrix synthesis and suppresses hypertrophic differentiation of growth plate chondrocytes, but has little effect on cell proliferation in vitro and vivo. To investigate if the nicotinic effect is mediated by alpha7 nAChR, we used MLA, the specific antagonist of alpha7 nAChR. MLA clearly reversed the effect, as assessed by ALB-stained colonies (Figure 2C), suggesting the involvement of alpha7 nAChR in the effect of nicotine on growth plate chondrocytes.

Long-term (four months) effect of nicotine on growth plate chondrocytes in alginate beads

Different from the case with agarose gel, human chondrocytes hardly proliferate in alginate beads, maintaining chondrocyte properties for more than eight months [19]. Moreover, molecular analysis can be done easily compared with that in agarose gel, since chondrocytes can be recovered from beads by chelation of divalent ions with ethylenediamine tetraacetic acid (EDTA) followed by centrifugation. We investigated the long-term effect of nicotine on growth plate chondrocytes by employing alginate bead culture. Chondrocytes encapsulated in alginate beads remained viable during the culture period (four months) in their lacunae. Nicotine did not affect viability of the chondrocytes at any indicated concentration. Nicotine dose-dependently suppressed ALB- and Safranin-O-stained areas at four months (Figure 3A).

To investigate expression of chondrocyte-specific genes, we performed RT-PCR analysis on chondrocytes in alginate beads. Genes for collagen type II (Col II), Aggrecan, collagen type X (ColX), ALP, and indian hedgehog (Ihh) were up-regulated at three weeks after the start of alginate bead culture (Figure 3B). In contrast, genes for parathyroid hormone receptor type I (PTHR1), matrix metalloproteinase type 13 (MMP13), vascular endothelial growth factor (VEGF), and Sox9 were constitutionally expressed and their expression level remained unchanged. We then performed RT-PCR analysis to investigate the expression of chondrocyte-specific genes in chondrocytes treated by nicotine for four months. Nicotine dose-dependently decreased the expression of Col II, Aggrecan, Col X, ALP, and Ihh gene (Figure 3C). These findings suggest that nicotine suppresses matrix synthesis and hypertrophic maturation of chondrocytes in long-term culture using alginate beads.

Functional calcium imaging

To investigate the intracellular signals after nicotinic stimulation, we performed calcium imaging assay for primary chondrocyte cultures, since alpha7 nAChR has large Ca^{2+} permeabilities and also induces elevated intracellular free calcium by releasing intracellular calcium stores [17]. Nicotine elicited a transient increase of intra-cellular calcium (Figure 4A) in a concentration-dependent manner (Figure 4B). MLA, the specific antagonist of alpha7 nAChR, inhibited the calcium signals in a concentration-dependent manner (Figure 4C), implying that the effect of nicotine on chondrocytes is mediated through the alpha7 nAChR.

Maternal nicotine exposure in wild-type mice

To study the effect of nicotine on endochondral ossification in vivo, ovulation-controlled pregnant C57BL/6J mice were given drinking water with or without nicotine during pregnancy, and skeletal growth of their fetuses was observed. At noon on gestational day 15, fetuses were surgicallly obtained and their legs were sectioned for measurement of the femur length (FL) and the length of the hypertrophic zone of the femur (HL) (Figure 5A). There were no significant differences of the amount of water consumed between nicotine-exposed group and control group. Maternal nicotine exposure significantly reduced the FL (Figure 5B) and HL/FL (Figure 5C) of mice at embryonic day 15.5 (E15.5), suggesting that nicotine delayed endochondral ossification.

Maternal nicotine exposure in alpha7 nAChR-disrupted mice

To clarify an involvement of alpha7 nAChR in nicotine-induced delayed skeletal growth in vivo, we investigated the effect